

1 Volatile (H₂O, CO₂, Cl, S) budget of the Central American
2 subduction zone

3

4 Freundt A¹, Grevemeyer I¹, Rabbel W², Hansteen TH¹, Hensen C¹,
5 Wehrmann H¹, Kutterolf S¹, Halama R^{2,3}, Frische M¹

6

7 ¹ SFB 574, GEOMAR Helmholtz Centre for Ocean Research Kiel, Germany

8 ² SFB 574, Institute for Geosciences, Christian Albrechts University of Kiel, Germany

9 ³ Institute of Earth and Environmental Science, University of Potsdam, Germany

10

11 Corresponding author: afreundt@geomar.de, phone +494316002131, fax +494316002924

12

13 Abstract

14 After more than a decade of multidisciplinary studies of the Central American
15 subduction zone mainly in the framework of two large research programmes,
16 the US MARGINS program and the German Collaborative Research Centre
17 SFB 574, we here review and interpret the data pertinent to quantify the
18 cycling of mineral-bound volatiles (H₂O, CO₂, Cl, S) through this subduction
19 system. For input flux calculations, we divide the Middle America Trench into
20 four segments differing in convergence rate and slab lithological profiles, use
21 the latest evidence for mantle serpentinization of the Cocos slab approaching
22 the trench, and for the first time explicitly include subduction erosion of forearc
23 basement. Resulting input fluxes are 40-62 (53) Tg/Ma/m H₂O, 7.8-11.4 (9.3)
24 Tg/Ma/m CO₂, 1.3-1.9 (1.6) Tg/Ma/m Cl, and 1.3-2.1 (1.6) Tg/Ma/m S -
25 (bracketed are mean values for entire trench length).

26 Output by cold seeps on the forearc amounts to 0.625-1.25 Tg/Ma/m H₂O
27 partly derived from the slab sediments as determined by geochemical
28 analyses of fluids and carbonates. The major volatile output occurs at the
29 Central American Volcanic Arc (CAVA) that is divided into 10 arc segments by
30 dextral strike-slip tectonics. Based on volcanic edifice and widespread tephra
31 volumes as well as calculated parental magma masses needed to form
32 observed evolved compositions, we determine long-term (10⁵ years) average
33 magma and K₂O fluxes for each of the 10 segments as 32-242 (106) Tg/Ma/m
34 magma and 0.28-2.91 (1.38) Tg/Ma/m K₂O - (bracketed are mean values for
35 entire CAVA length). Volatile/K₂O concentration ratios derived from melt
36 inclusion analyses and petrologic modelling then allow to calculate volatile
37 fluxes as 1.02-14.3 (6.2) Tg/Ma/m H₂O, 0.02-0.45 (0.17) Tg/Ma/m CO₂, 0.07-
38 0.34 (0.22) Tg/Ma/m Cl. The same approach yields long-term sulfur fluxes of
39 0.12-1.08 (0.54) Tg/Ma/m while present-day open-vent SO₂-flux monitoring
40 yields 0.06-2.37 (0.83) Tg/Ma/m S.
41 Input-output comparisons show that the arc water fluxes only account for up
42 to 40% of the input even if we include an "invisible" plutonic component
43 constrained by crustal growth. With 20-30% of the H₂O input transferred into
44 the deeper mantle as suggested by petrologic modeling, there remains a
45 deficiency of, say, 30-40% in the water budget. At least some of this water is
46 transferred into two upper-plate regions of low seismic-velocity and electrical-
47 resistivity whose sizes vary along arc: one region widely envelopes the melt-
48 ascent paths from slab-top to arc, the other extends obliquely from the slab
49 below the forearc to below the arc. Whether these reservoirs are transient or
50 steady remains unknown.

51

52 Keywords:

53 subduction input, forearc dewatering, arc magmatism, subduction fluids

54

55 **1. Introduction**

56 The fluxes of volatiles and fluids into, and out of, subduction zones are a

57 major component of the global volatile elemental exchange between

58 lithosphere, hydrosphere and atmosphere that affects long-term changes in

59 climate and environmental conditions for the biosphere and relates to

60 questions such as the permanence of the ocean through geologic time.

61 Tropospheric through stratospheric emissions of volcanic gases can have a

62 variety of severe environmental impacts on regional to global scales (Delmelle

63 et al. 2002; Robock 2000; Metzner et al. this volume; von Glasow et al. 2009;

64 Kutterolf et al. 2013). Volcanic CO₂ emissions are particularly important for the

65 evolution of the atmosphere's composition over geological time scales

66 (Hansen and Wallmann 2003). Moreover, fluxes of fluids and of mineral-

67 bound volatiles associated with mechanical and metamorphic transformation

68 processes change rheological and thermodynamic properties in the

69 subduction system and ultimately pre-determine the frequency and intensity of

70 geohazards such as earthquakes and explosive volcanic eruptions.

71

72 Subduction zones and mid-ocean ridges are the major sites of material

73 exchange between the deeper mantle and the lithosphere and surface, where

74 the exchange of volatile components is particularly important for the

75 biosphere. In order to understand to what extent the output at mid-ocean

76 ridges is balanced by return flux into the deeper mantle at subduction zones,
77 the budget between subduction input and output needs to be determined for
78 each volatile species. In one of the first attempts to budget global subduction
79 fluxes, Peacock (1990) estimated that only 10% of subducted H₂O and CO₂
80 returns to the surface via arc magmatism. More recently, comprehensive
81 analyses of modern subduction zones by Jarrard (2003), Hacker (2008) and
82 van Keken et al. (2011) revealed large regional differences in subduction
83 fluxes of volatile components. Return fluxes of H₂O into the deep mantle have
84 been estimated by advanced thermal and petrologic modeling of slab
85 dehydration (Rüpke et al. 2004; Hacker 2008; van Keken et al. 2011;
86 Faccenda et al. 2012) while various approaches were used to quantify the
87 global arc-volcanic volatile outputs (e.g., Marty and Tolstikhin 1998; Hilton et
88 al. 2002; Straub and Layne 2003; Wallace 2005; Fischer 2008; Ruscitto et al.
89 2012). However, considerable uncertainties remain in these budgets due to
90 quite incomplete knowledge of subduction input conditions and the mass
91 fluxes at the arcs. While the serpentinization of subducted mantle (Peacock
92 2001) has been considered in the most recent studies (Hacker 2008; van
93 Keken et al. 2011; Halama et al. this volume), the extent of serpentinization at
94 individual subduction zones is mostly poorly constrained. None of the
95 budgeting studies has considered subduction-erosion of forearc crust (von
96 Huene and Scholl 1991) as an input component. Thus there is a continued
97 demand for comprehensive analyses of individual subduction zones.
98
99 The Central American subduction system, and in particular the Costa Rican
100 and Nicaraguan segments, has been a focus of multi-disciplinary research

101 during the past decade, led by two major research programmes: the German
102 Collaborative Research Center SFB 574 and the US MARGINS program. The
103 combination of offshore and onshore geophysical observations, submarine
104 investigations of forearc fluid venting, petrological analyses of subduction-
105 zone metamorphic complexes over the whole range of P-T conditions,
106 volcanological/geochemical studies of arc magmatism and advanced
107 geodynamic numerical modelling allow us to constrain the sources and sinks
108 of volatiles, and the fluxes between them. In this paper we review the present
109 knowledge about the fate of volatiles (H₂O, CO₂, Cl, S) in the Central
110 American erosive subduction zone which is transitional from an oceanic
111 nature in the south to a continental nature in the north. We attempt to
112 calculate volatile budgets whereby the recognition of serpentinization of slab
113 upper mantle, the quantification of subduction-erosion rates, and the
114 comprehensive determination of arc-magma fluxes are particularly important
115 factors. A companion paper (Völker et al. this volume) summarizes data on
116 the accretionary, continental subduction zone of southern Chile.

117

118 2. The Central American subduction zone

119 The oceanic Cocos plate subducts beneath the Caribbean plate along the
120 Middle America Trench (MAT) that is paralleled on land by the Central
121 American Volcanic Arc (CAVA) extending from Costa Rica to Guatemala (Fig.
122 1). The Cocos plate from Nicaragua to Guatemala, northwest of the triple-
123 junction trace, is composed of normal MORB produced at the East Pacific
124 Rise but Cocos plate offshore Costa Rica stems from the Cocos-Nazca
125 spreading center when it was close to the Galapagos hotspot (Mann et al.

126 2007). This part of the Cocos plate is straddled by numerous seamounts in a
127 northern stripe, followed by the Cocos Ridge to the south (Fig. 1). The Cocos
128 Plate subducts at 62 to 78 km/Ma and its sub-arc dip varies widely from ~44°
129 at southern Costa Rica through ~65° at Nicaragua to ~55° at Guatemala
130 (Syracuse and Abers 2006); consequently sub-arc depth to the slab top is
131 largest at Nicaragua. The volcanic front, which assumed its present position
132 about 8 Ma ago (Ehrenborg 1996), is divided into 10 segments (Fig. 1) by
133 dextral strike-slip tectonics caused by slightly oblique subduction (Carr 1984;
134 DeMets 2001). Arc magmatic compositions vary systematically with latitude in
135 response to changing subduction conditions (Carr et al. 2003, 2007;
136 Feigenson et al. 2004; Hoernle et al. 2002; Patino et al. 2000) as well as arc-
137 parallel mantle flow (Hoernle et al. 2008; Rabbel et al. 2011). The upper-plate
138 crust gets as thin as 30 km in Nicaragua while it is around 38 km in northern
139 Costa Rica with a largely basaltic composition; the crust thickens through El
140 Salvador to 43 km in Guatemala while changing to a felsic, continental
141 composition (Lücke this volume; Kim et al. 1982; Carr 1984; Walther et al.
142 2000; MacKenzie et al. 2008).

143

144 **3. Input into the subduction zone**

145 In this section we investigate the H₂O, CO₂, Cl, and S fluxes associated with
146 each of the lithological units of the subducting slab in order to determine the
147 total input fluxes. The volatile components are transported both dissolved in
148 pore water and structurally bound in mineral phases. The pore water, which is
149 most abundant in the marine sediments, is largely expelled by tectonic
150 compression during the first few kilometers of subduction to escape through

151 the prism toe and forearc (Jarrard 2003; Saffer 2003; Hensen and Wallmann
152 2005; Saffer and Tobin 2011). Here we ignore pore water and its dissolved
153 components and determine input fluxes only for the mineral-bound volatile
154 components in the different subducted lithologies: sediments, igneous oceanic
155 crust, serpentized oceanic mantle, and eroded upper-plate crust.
156 In the following we determine the input volatile mass fluxes (F_v) per unit length
157 of the subduction zone by the volatile concentration (C_v) in each rock unit, the
158 thickness (H) and density (ρ) of that unit adjusted for pore space (ε), and the
159 subduction rate (V_c) as

160

161 $F_v = C_v H (1 - \varepsilon) \rho V_c.$

162

163 Table 1 summarizes the calculation parameters and results for the different
164 slab lithologies.

165

166 3.1. Sediments

167 Jarrard (2003) has quantified the volatile input by subducted sediments at
168 Central America updating earlier work by Plank and Langmuir (1998). DSDP
169 site 495 and ODP site 1039 show that sediment on the incoming plate from
170 Guatemala to Costa Rica comprises about 150 m hemipelagic clays underlain
171 by about 250 m pelagic carbonates; thus carbonate contents vary vertically
172 between 1 to 87% (Li and Bebout 2005). Large variations in clay and
173 carbonate thicknesses occur on the topographically rough seafloor off Costa
174 Rica (Spinelli and Underwood 2004). Jarrard (2003) calculated the weight
175 fractions in the total sediment pile of pore water (48.7 wt%), mineral-bound

176 water (4.59 wt%), and CO₂ (26.55 wt%). He also estimated chloride contents
177 in pore water assumed to have seawater composition. However, chloride
178 dissolved in pore water or stored in soluble salts will be quickly lost from the
179 subduction system with the expelled pore water. We prefer insoluble mineral-
180 bound chloride concentrations measured by ion chromatography after
181 pyrohydrolysis of DSDP site 495 sediment samples (for analytical procedures
182 see John et al. 2011), giving 810-2273 ppm Cl in the overlying clays and 82-
183 368 ppm Cl in the underlying carbonates. The depth-averaged concentration
184 of insoluble mineral-bound Cl is 805 ppm. The average sulfur content of
185 pelagic clay at ODP site 1039 is 5320 ppm whereas there is virtually no sulfur
186 in the underlying carbonate (Kimura et al. 1997); the average sulfur content
187 over the entire sediment column is thus 1900 ppm.

188

189 3.2. Cocos plate igneous crust

190 Jarrard (2003) has analyzed in detail the lithological units of extrusive and
191 intrusive oceanic crust for their volatile-carrying capacities, mainly as a
192 function of age. We use his Central America data to calculate pore water
193 (0.91 wt%), mineral-bound water (1.28 wt%) and CO₂ (0.18 wt%)
194 concentrations depth-averaged over the crustal thickness of 5 km offshore
195 Nicaragua through Guatemala (Walther et al. 2000; von Huene et al. 1980) to
196 7 km offshore Costa Rica (Weinrebe and Flüh 2002). Seismic refraction data
197 shows profoundly reduced seismic velocities within and below seamounts
198 offshore Costa Rica (Ivandić et al. 2010), suggesting more intense hydration
199 of crust heavily populated with seamounts compared to the smooth Cocos
200 seafloor further north (Fig. 1) but this is yet difficult to quantify.

201

202 Jarrard's chloride estimate is again based on pore water; we here prefer
203 measured chlorine contents of altered MORB. Bonifacie et al. (2007) did not
204 leach their altered MORB samples prior to analysis such that their bulk Cl
205 contents of 240-490 ppm include Cl bound in soluble phases (salts) and Cl
206 bound in non-soluble silicate minerals. Own analyses involving leaching of the
207 sample-powders yielded 20-37 ppm insoluble Cl in oceanic crust offshore
208 Guatemala (samples DSDP/67/495/48R/04W/82-84 and
209 DSDP/67/500/19R/01W/20-27) comparable to concentrations of 12-54 ppm Cl
210 found for Izu-Bonin and Nankai (samples ODP/185/1149B/32R/01W/60-63
211 and IODP/322/C0012A/57R/01W/51-56). The respective bulk chlorine
212 contents were 65-144 ppm and 185-1189 ppm such that Cl bound in non-
213 soluble silicate minerals only accounts for 5-30% of the total Cl subducted
214 with the crust. Depending on when pervading fluids scavenge soluble Cl from
215 the crustal rocks relative to metamorphic phase changes of the Cl-bearing
216 silicates, soluble and insoluble Cl may be fractionated from each other and
217 follow different paths through the subduction system. However, this has not
218 yet been systematically studied and is a subject beyond the scope of this
219 contribution. Since we are mainly concerned with a bulk subduction zone
220 volatile budget, we use the total Cl content (soluble plus insoluble) of ocean
221 crust estimated as 300 ppm in the flux calculations.

222

223 Sulfur contents of fresh MORB range between 800 and 1400 ppm (Wallace
224 and Anderson 2000), and vesicular, partly degassed volcanic glasses on the
225 Cocos ridge and associated seamounts have sulfur contents of 300-1000

226 ppm, in contrast to 1300-1700 ppm found in dense, undegassed
227 hyaloclastites of the Fisher ridge offshore Costa Rica (Werner et al. 1999).
228 Judging from Troodos ophiolite analyses (Alt 1994), high-temperature
229 seawater alteration of oceanic crust seems to mainly redistribute sulfur from
230 the lower intrusives to the upper crust with little net change in the overall
231 sulfur content while subsequent low-temperature alteration removes some
232 sulfur from the upper extrusives. We estimate an average concentration of
233 1000 ppm S of the subducting Cocos plate crust but note the large uncertainty
234 associated with this value.

235

236 3.3. Serpentinized mantle

237 Water

238 High-resolution bathymetry and seismic profiles show intense bend-faulting of
239 the Cocos plate across the outer rise (Fig. 1) with many faults extending into
240 mantle depths that may have provided pathways for deeply intruding water
241 (Ranero et al. 2003; Ranero and Weinrebe 2005). Upper-mantle velocity
242 anomalies revealed by seismic tomography, and heat-flow measurements,
243 imply large amounts of water carried by serpentinized mantle (Abers et al.
244 2003; Grevemeyer et al. 2005, 2007). Subsequent studies, however, show
245 that some of the velocity anomaly must be attributed to the presence of faults,
246 and that the depth range of hydration is limited by the change from tensional
247 to compressional stress conditions downward in the bending plate (Lefeldt
248 and Grevemeyer 2008; Lefeldt et al. 2009, 2012). Moreover, seismic
249 velocities might be influenced by anisotropy related to bend faulting although
250 such anisotropy has not yet been clearly demonstrated by refraction profiles.

251 Therefore water contents derived from seismic velocity reduction should be
252 considered maximum values. In trench-perpendicular seismic profiles offshore
253 Nicaragua, Ivandic et al. (2008, 2010) observed an increasing extent of
254 mantle hydration with approach toward the trench (Fig. 2), and concluded that
255 the upper 3.5 km of the Cocos-plate mantle reaching the trench are 12-17%
256 serpentinized, implying a bulk-rock water content of about 2 wt% H₂O. Van
257 Avendonk et al. (2011) analyzed seismic velocity variations in the incoming
258 plate along the trench offshore southern Nicaragua and northern Costa Rica
259 (Fig. 2). Offshore Nicaragua they found some along-trench variation in the
260 degree of serpentinization of Cocos plate mantle but estimate an average
261 water content of 3.5 wt% in the upper roughly 7 km of the mantle.
262 Offshore Costa Rica, however, where the Cocos plate crust is thickened by the
263 Galapagos hotspot track (Cocos Ridge and seamount province; Fig. 1), slab
264 buoyancy only allows for little bending (Ranero and Weinrebe 2005). Here,
265 seismic refraction data provide much faster velocities ($V_P=7.8$ km/s) in the
266 upper mantle north of Cocos Ridge (Walther 2003; Walther and Flueh 2002).
267 These were supported by the recent along-trench investigations of van
268 Avendonk et al. (2011) who show an increase in seismic velocities,
269 interpreted as a steep decrease in upper-mantle water contents, from
270 southern Nicaragua to central Costa Rica (Fig. 2). Other seismic refraction
271 and wide-angle investigations on the Cocos plate along profiles normal to the
272 margin yielded 8.1 km/s for the mantle on three sections off Costa Rica (Ye et
273 al. 1996), 8.0 km/s northwest of Osa peninsula (Stavenhagen et al. 1998),
274 and 8.1 km/s northwest of Nicoya peninsula (Christeson et al. 1999; Sallares
275 et al. 2001). Using these values we estimate that the mantle offshore of Costa

276 Rica is much less hydrated than offshore of Nicaragua. The degree of
277 serpentinization might be variable, ranging from 0% to ~10% of
278 serpentinization. Thus, bound water contents will be ≤ 1 wt% and limited to the
279 uppermost 1-3 km of the mantle.
280 The seismological observations at Nicaragua have been used to calibrate a
281 numerical reactive-flow model of outer-rise mantle serpentinization (Iyer et al.
282 2012) that uses temperature-dependent reaction rates (between 100-400°C
283 with maximum at 270°C), plate temperature as a function of plate age, and a
284 linear increase in porosity toward the trench simulating the effect of bend
285 faulting. Next to reaction kinetics, plate age and convergence rate (i.e. the
286 time from onset of bend faulting to subduction at the trench) are the major
287 controlling factors on the degree of slab mantle serpentinization. Application
288 of this model to Central America (K. Iyer, pers. comm. 2012) shows that the
289 expected slab mantle water contents are very similar from Nicaragua through
290 El Salvador to Guatemala but lower at Costa Rica as observed seismically. In
291 our flux calculations for serpentinized mantle we use 3 wt% H₂O for Nicaragua
292 to Guatemala and 1 wt% H₂O for Costa Rica (Table 1).

293

294 Carbon dioxide

295 The highly variable carbon contents of serpentinites are controlled by parent-
296 rock composition, by hydrothermal alteration and, near the seafloor, by
297 microbial activity depositing organic carbon. In ultramafic hydrothermal
298 systems carbonate may precipitate from pure seawater, from heating of
299 seawater and from cooling of hydrothermal fluids (Eickmann et al. 2009; Bach
300 et al. 2011). Analyzed serpentinites from a wide range of settings and

301 formation conditions (but none from outer-rise bend faulting) contain 60 to
302 3000 ppm CO₂ although veined rocks may have wt-%-contents (Delacour et
303 al. 2008a; Alt et al. 2013). Since geophysical studies limit serpentinization to
304 <17% at the Middle America Trench, we adopt a value of 200 ppm CO₂.

305

306 Chlorine

307 Scambelluri et al. (2004) determined 729 ppm Cl as an average value of
308 oceanic serpentinite and showed how this concentration gradually decreases
309 to 45 ppm Cl in high-pressure olivine-orthopyroxene rocks as a consequence
310 of metamorphic slab dehydration. Kendrick et al. (2013) determined 990-2300
311 ppm Cl in 93-99% serpentinized rocks at the Guatemalan forearc but their
312 global seafloor-serpentinites data set shows <700 ppm Cl at <60%
313 serpentinization as expected at the Middle America Trench. The analyses of
314 Scambelluri et al. and Kendrick et al. did not include prior thorough leaching
315 and give bulk (soluble plus insoluble) Cl concentrations. Pre-subduction
316 serpentinites analyzed by John et al. (2011) with prior leaching have
317 concentrations of 120-350 ppm of insoluble, silicate-bound Cl. Serpentinites
318 from the Hess Deep contain 900-5100 ppm (average 2524 ppm) water-
319 soluble chloride stored in salt minerals in addition to 300-1200 ppm (average
320 535 ppm) insoluble Cl stored in other minerals (Barnes and Sharp 2006).
321 Obviously there is a wide margin of uncertainty in estimating the Cl
322 concentration of serpentinite subducted at the Middle America Trench and, as
323 discussed for ocean crust in chapter 3.2, the fate of soluble versus insoluble
324 Cl as the serpentinite dives to high pressures and temperatures remains
325 unclear. Kendrick et al. (2012) argue that a significant fraction of Cl in

326 serpentinite is subducted beyond sub-arc depths. In the flux calculations we
327 use 1000 ppm Cl as a conservative estimate of the bulk Cl content but it may
328 also be considered as an upper bound of insoluble Cl content.

329

330 Sulfur

331 The combined data of serpentinized harzburgites from the Hess Deep at the
332 western end of the Cocos-Nazca spreading center (Alt and Shanks 1998) and
333 the Mariana forearc (Alt and Shanks 2006) show sulfur contents similar to
334 fresh harzburgite (<200 ppm) at <50% serpentinization; up to 860 ppm S are
335 only reached at higher degrees of serpentinization. Oceanic serpentinites
336 formed at slow-spreading centers may even reach 1 wt% sulfur concentration
337 (Alt and Shanks 2003; Alt et al. 2013; Delacour et al. 2008b). Here we
338 assume an average concentration of 200 ppm S (similar to little altered
339 harzburgite; Puchelt et al. 1996) for the only moderately serpentinized
340 uppermost mantle of the subducting Cocos plate.

341

342 3.4. Subduction erosion

343 Subduction erosion, i.e. the subduction of material scraped off the base of the
344 overlying plate, occurs at a large fraction of the global subduction-zone length
345 (von Huene and Scholl 1991) and is another process introducing volatile
346 components into the subduction system. Subduction erosion mainly operates
347 underneath the continental slope promoted by hydrofracturing caused by
348 overpressured water released from the subducted sediments (Ranero et al.
349 2008). Modeling suggests that subduction erosion occurs when forearc
350 sediments have high rheological strength, i.e. are less weakened by fluids

351 (Gerya 2011; Gerya and Meilick 2010). Subduction erosion occurs along the
352 entire Central American subduction zone but the detailed processes and rates
353 vary (Ranero and von Huene 2000; Ranero et al. 2000). Where the smooth
354 Cocos plate ocean floor subducts beneath Guatemala (Fig. 1), Vannucchi et
355 al. (2004) determined an erosion rate of about $12 \text{ km}^3/\text{Ma}/\text{km}$. In contrast,
356 where the Cocos ridge and seamount province subduct beneath Costa Rica
357 (Fig. 1), subduction erosion is much more efficient with $113 \text{ km}^3/\text{Ma}/\text{km}$ for
358 about the past 6.5 Ma (Vannucchi et al. 2003). For the time span back to 17
359 Ma, the average erosion rate was $35 \text{ km}^3/\text{Ma}/\text{km}$ (Vannucchi et al. 2001). The
360 dramatic increase in erosion rate thus roughly coincides with the Pliocene
361 onset of subduction of the Cocos Ridge (Hoernle et al. 2002).

362

363 The nature of the material subducted by erosion is difficult to determine.
364 Based on geophysical evidence and ODP drilling results, Vannucchi et al.
365 (2001) conclude that the forearc basement eroded off Costa Rica corresponds
366 to the geological structure of the Nicoya peninsula, which is formed by a
367 basement of accreted and brecciated ocean crust overlain by marine
368 sediments of Late Cretaceous through Eocene age. Similarly, Azema et al.
369 (1982) interpreted seismic profiles to show stacked ophiolitic slabs forming the
370 forearc basement off Guatemala. Walther et al. (2000) identified accreted
371 oceanic crust as the forearc basement offshore Nicaragua. Ages of accreted
372 complexes range from 20 to 70 Ma (Hoernle et al. 2002). Thus the material
373 subducted by erosion from Costa Rica through Guatemala seems to have a
374 dominant composition similar to strongly altered oceanic crust. As an
375 approximation, we thus estimate mineral-bound volatile contents as 3.57 wt%

376 H₂O and 0.54 wt% CO₂ (mean values for 20-70 Ma old oceanic crust after
377 Jarrard 2003). We estimate 300 ppm Cl and 1000 ppm S in the eroded
378 material as in Cocos plate crust (see 3.2).

379

380 3.5. Input fluxes along the subduction zone

381 The average calculated subduction input fluxes of the mineral-bound volatiles
382 at Central America are 53 Tg/Ma/m H₂O, 9.3 Tg/Ma/m CO₂, 1.6 Tg/Ma/m Cl,
383 and 1.6 Tg/Ma/m S (Table 1), such that the typical composition of the bulk
384 subducted volatile mass is approximately 81% H₂O, 14% CO₂, and 2.5% Cl
385 and 2.4% S (ignoring other volatiles such as F, Br, N, etc.). The input fluxes of
386 mineral-bound water, CO₂, Cl and S gradually increase from Guatemala to
387 Nicaragua mainly in response to increasing convergence rate since there is
388 no indication of major changes in subducted lithology (Fig. 3). Toward Costa
389 Rica, however, H₂O and Cl input fluxes drop because the Cocos plate mantle
390 is very little serpentinized (Fig. 3). In contrast, thicker Cocos Plate oceanic
391 crust, high rates of subduction erosion and faster convergence cause an
392 increase in S and CO₂ subduction.

393 The input of mineral-bound water is dominated by serpentinized mantle (Fig.
394 4a), except at Costa Rica where ocean crust and subduction-erosion are the
395 main water carriers. For comparison, published globally averaged distributions
396 of water fluxes across the lithologies are shown by arrows in Fig. 4a; while our
397 data for Costa Rica are similar except for the stronger role of subduction
398 erosion, our results for Nicaragua through Guatemala suggest that mantle
399 serpentinite is much more important than igneous crust as a water carrier.

400 More than 60% of subducted CO₂ is carried by the sediments (Fig. 4b) while
401 ocean crust delivers another 20-30%. The crust also carries about 20% of
402 subducted chlorine but the Cl input is clearly dominated by about 80% riding
403 with the serpentinite (except at Costa Rica). This is distinctly different from
404 Jarrard (2003) who had the sediments as the major carrier of chlorine (Fig.
405 4c) because he considered chlorine in pore water rather than mineral-bound
406 chlorine as done here, and he did not consider serpentinitized mantle as a
407 chlorine carrier.

408 The subduction input of sulfur is largely dominated (>70%) by the subducted
409 ocean crust (Fig. 4d). Thus the uncertainties that most affect the flux
410 estimates are those of water contents in crust and serpentinite, CO₂ contents
411 in sediments, chlorine contents in serpentinite, and sulfur contents in the
412 crust. Uncertainty in the nature of material eroded from the forearc plays a
413 role at Costa Rica but is less important along the remaining subduction zone.
414 These potential errors in volatile concentrations translate directly into relative
415 errors in the flux calculations and are larger than relative uncertainties in the
416 physical subduction parameters.

417

418 4. Output at the forearc

419 Fluid seepage at the Central American forearc is focussed at a variety of
420 structures such as mud volcanoes, mud domes, faults, and scarps formed by
421 seamount subduction. High-resolution bathymetric, geophysical and
422 geochemical studies as well as video observations have identified more than
423 100 fluid seep sites at the forearc of Costa Rica and Nicaragua, which are
424 typically concentrated at mid-slope depths (Fig. 5; Sahling et al. 2008; Ranero

425 et al. 2008). Discharging fluids are generally rich in methane feeding bacterial
426 and other organic vent communities that act as a benthic filter limiting
427 methane outflow into the ocean bottom water (Linke et al. 2005; Karaca et al.
428 2010, this volume; Suess this volume). Measured CH₄ fluxes vary significantly
429 over time scales of months to years (Mau et al. 2006, 2007, this volume).
430 Moreover, geologic records show that the seepage activity of mud mounds
431 varies spatially and temporally on time scales of 10³ to 10⁵ years (Liebetrau et
432 al. this volume; Mörz et al. 2005; Kutterolf et al. 2008). The largest outflow
433 rates have been determined for seep sites at seamount-subduction scarps
434 offshore Costa Rica (Mau et al. this volume) but the density of seeps is larger
435 offshore Nicaragua (Fig. 5).
436 Seismic profiles show that mounds and other cold seeps are underlain by
437 relatively undeformed slope sediment and likely fed by fault-controlled fluid
438 pathways which may originate at the plate boundary several kilometers below
439 the seafloor (Ranero and von Huene 2000; Hensen et al. 2004; Schmidt et al.
440 2005). Fluid movement near the plate boundary and through the forearc is
441 associated with pore pressure change (Saffer 2003) and may cause seismic
442 swarm activity which was indeed observed offshore Nicaragua (Thorwart et al.
443 this volume). Emanating fluids are diluted with respect to seawater by mixing
444 with freshwater derived from smectite to illite transformation as shown by
445 δ¹⁸O-δD systematics of fluid endmembers (Hensen et al. 2004) and
446 thermogenically formed CH₄ in the mound fluids (Schmidt et al. 2005). The
447 most likely source of that freshwater is the subducted hemipelagic sediment,
448 because it is rich in detrital smectite (Spinelli and Underwood 2004) from
449 terrestrial weathering, other than at high-latitude margins where authigenic

450 smectite yields a more limited freshwater reservoir (Scholz et al. 2013).
451 Moreover, temperatures of 60-150°C required for the smectite to illite
452 transformation are typically not reached inside the continental slope but within
453 the sediments at the plate boundary (Fig. 5; Ranero et al. 2008). Elevated
454 $\delta^{18}\text{O}$ values of mound carbonates indicate that the supply of deep-seated
455 fluids is a long-term process (Han et al. 2004; Mavromatis et al. this volume;
456 Liebetrau et al. this volume; Suess this volume). However, expelled fluids
457 have a geochemical signature that shows also evidence for various types of
458 fluid-rock interaction processes during the ascent. Thus, the $^{129}\text{I}/\text{I}$ fluid ages of
459 ≥ 25 Ma (Lu et al. 2007) are inconsistent with the fluid directly derived from the
460 subducting sediments but rather require an additional source such as iodine
461 released from old sediments of the wedge.

462 The average density along the Costa Rica - Nicaragua margin is one seep
463 every 4 km. Based on seep-flux measurements, Ranero et al. (2008)
464 estimated an average fluid flow rate per seep/mound of 0.5-1.0 cm/yr that
465 corresponds to an average present-day discharge of 2500-5000 m³/yr per 4
466 km equivalent to 0.625-1.25 Tg/Ma/m (per unit trench length). Saffer (2003)
467 investigated porosity and pore pressure variations at the Costa Rica forearc
468 and deduced a dewatering rate of underthrust sediment of 8 Tg/Ma/m across
469 the first 1.6 km of subduction, corresponding to 65% of subducted sediment
470 pore water. Moore et al. (2011) show that this rate of pore water drainage for
471 the erosive Costa Rican margin is much more rapid than at the accretionary
472 Nankai margin. Moreover, this flux is 6-13 times the flux estimated from
473 measurements at the mid-slope seeps some 20-30 km from the trench, but
474 much of it is typically lost by bedding-parallel backflow and hence, would not

475 be available as a source for seep fluids. The 0.625-1.25 Tg/Ma/m seep flux
476 would account for 58-116% of the input flux of mineral-bound water in the
477 sediment but a significant fraction of mineral-bound water must be retained in
478 the sediments because high-pressure metasediments typically contain OH-
479 bearing minerals up to pressures and temperatures well beyond the sub-
480 forearc (Domanik and Holloway 1996; Bebout et al. 2007; Hacker 2008).
481 Hence, while containing freshwater from the smectite to illite transformation, a
482 significant fraction of the seep flux must derive from pore water of subducting
483 sediment and/or, more likely, the overlying forearc wedge. Nevertheless, even
484 ignoring the contribution of pore water, the seep output of 0.625-1.25
485 Tg/Ma/m only accounts for $\leq 2\%$ of the total mineral-bound water input with the
486 subducting slab.

487

488 Freshened fluids emanating at the slope most likely originate from subducting
489 sediments but have become strongly modified by fluid-rock interactions during
490 passage through the forearc wedge (Suess this volume) which make it
491 impossible to derive quantitative estimates for slab-sediment-derived fluxes of
492 CO₂, S and Cl through the forearc. Methane and CO₂ are likely to be
493 produced in the subducting sediments within the temperature window of the
494 smectite to illite transformation as suggested by findings of thermogenic
495 methane in seep fluids (Schmidt et al. 2005). However, typically components
496 from biogenic and thermogenic sources are mixed (C. Hensen, unpublished
497 data) such that exact quantities are difficult to assign. Carbon stored in
498 carbonates is stable at P-T-conditions of subducting sediments below the
499 forearc and cannot contribute to C-fluxes to the forearc. Similarly, pyrite and

500 other Fe-sulphides are also stable at these conditions such that mineral-
501 bound sulfur will not be lost. Moreover, a loss of pore-water sulphate to the
502 forearc is also unlikely as it is quantitatively reduced by anaerobic oxidation of
503 methane (Hensen and Wallmann 2005) and subsequently precipitated as iron
504 sulphides. The net loss of Cl to the forearc wedge through seepage is difficult
505 to assess as it depends on the mixing ratio between available pore water at
506 depth and clay-mineral derived water. Since pore water of normal salinity may
507 be taken up elsewhere along the flow path, the initial concentration of Cl
508 cannot be reconstructed. However, compared to the large loss of Cl with pore
509 water due to tectonic compression close to the deformation front, the
510 contribution from mineral-bound (soluble or insoluble) chlorine can most likely
511 be neglected.

512

513 5. Output at the volcanic arc

514 The volcanic arc is the major site of volatile output of the subduction zone.
515 Silicate melts originating in the mantle wedge metasomatized by slab-derived
516 fluids carry dissolved volatiles into crustal levels where they become partly
517 stored in plutonic rocks but mostly exsolve during magma storage and during
518 eruptions, and are largely transferred into the atmosphere. In the following, we
519 apply two approaches to estimate volatile fluxes from the mantle wedge to the
520 volcanic front: (1) long-term average fluxes based on erupted magma
521 volumes and associated melt compositions, and (2) present-day fluxes based
522 on measurements at continuously degassing volcanoes.

523

524 5.1. Long-term magma and volatile fluxes

525 Magma fluxes

526 In order to determine volatile fluxes from the arc via volcanic eruptions, both
527 the erupted magma masses and the respective volatile concentrations need
528 to be known. Carr (1984) and Carr et al. (1990, 2007) obtained long-term
529 average magma fluxes from CAVA volcanoes by measuring the volumes of
530 the volcanic edifices and constraining their age. Kutterolf et al. (2008)
531 extended that work by also including the magma masses stored in the widely
532 dispersed tephras formed by highly explosive eruptions, which account for
533 about half of the calculated total magma mass output of the arc. Erupted
534 magmas span a wide range in compositions from basalt through rhyolite, with
535 the widespread tephras mostly having evolved magmatic compositions. The
536 parental magma masses needed to form the observed differentiated
537 compositions by fractional crystallization can be calculated by geochemical
538 mass balance and are included in the total magma production of volcanic
539 activity. Kutterolf et al. (2008; their Fig. 6) show how the resulting magma
540 fluxes vary between individual volcanic centers along the volcanic front. Here
541 we simplify that data by calculating the long-term average magma flux for
542 each of the 10 tectonic segments of the arc (Fig. 1).

543

544 Volatile concentrations

545 Volatile concentrations in about 2500 melt inclusions and matrix glasses of
546 tephra samples collected along the entire CAVA have been determined by a
547 variety of methods in SFB 574. It is generally assumed that melt inclusions
548 represent the pre-eruptive volatile contents of melts while matrix glasses

549 contain the volatiles remaining after degassing to atmospheric pressure, such
550 that the concentration difference between both gives the volatile fraction
551 degassed into the atmosphere. This is a minimum assumption for poorly
552 soluble volatiles (CO₂, S) because they may have formed a separate fluid
553 phase already during entrapment of the melt inclusions.

554 Water contents were measured by ion probe and FTIR in melt-inclusion and
555 matrix glasses, and calculated from plagioclase-melt equilibrium compositions
556 after Putirka (2008) and Lange et al. (2009) as well as from amphibole
557 compositions after Ridolfi et al. (2010). CO₂ contents of primitive melt
558 inclusions have been measured by ion probe (Wehrmann et al. 2011) while S
559 and Cl contents have been mostly analyzed by electron microprobe.

560

561 Volatile/K₂O ratios

562 The more soluble volatiles (H₂O, Cl) are typically enriched like incompatible
563 elements during differentiation of magmas from basaltic to more evolved
564 compositions. Since potassium also behaves as an incompatible element in
565 the CAVA magmas (except in rare alkali feldspar-bearing rhyolites in
566 Guatemala), we have corrected for the fractionation effect by determining the
567 volatile/K₂O mass ratios. Using mass-weighted average bulk-rock K₂O
568 contents for each volcano, we have converted the erupted magma mass
569 fluxes along the arc to the respective K₂O mass fluxes which, when multiplied
570 by the respective volatile/K₂O mass ratios, yield the magmatic volatile mass
571 fluxes from the mantle to the surface. In the following, we investigate along-
572 arc variations in volatile/K₂O in order to derive the parameterizations used for
573 volatile flux calculations; typically these are upper envelopes of observed data

574 based on the assumption that reduced volatile/K₂O values in any magmatic
575 system result from volatile exsolution.

576

577 Water

578 In their study of primitive melt inclusions in basalt-hosted olivines along the
579 CAVA, Sadofsky et al. (2008) found H₂O contents to systematically increase
580 with Ba/La, a geochemical slab signature. H₂O/K₂O values measured in
581 primitive melt inclusions (Sadofsky et al. 2008; Wehrmann et al. 2011) reach
582 values up to 20 in Nicaragua but only up to 4.5 in Guatemala and 3.5 in Costa
583 Rica (Fig. 6a). The high values in Nicaragua come from samples of Cerro
584 Negro, Nejapa and Granada which are all very K-poor (avg. 0.19 wt% K₂O
585 resulting in avg. H₂O/K₂O=6.1), while maximum water concentrations exceed
586 those of other mafic CAVA suites by only up to 1 wt%. In contrast, samples
587 from Masaya have avg. 1.47 wt% K₂O and H₂O/K₂O=1 which is more
588 compatible with the range observed in central Nicaraguan felsic rocks.
589 H₂O/K₂O values in mafic melt inclusions of Guatemala and Costa Rica fit the
590 values of evolved tephras there. The fact that mafic compositions reach
591 higher maximum H₂O/K₂O values than felsic tephras is due to buffering of
592 dissolved H₂O at the saturation limit in many of the felsic compositions as
593 shown by the occurrence of aqueous fluid inclusions and thermobarometric
594 constraints. We therefore use an upper envelope of the H₂O/K₂O along-arc
595 variation (Fig. 6a) to calculate the magmatic water fluxes from the mantle to
596 the arc.

597

598 Carbon dioxide

599 CO₂ contents of primitive melt inclusions reach maximum values (≤ 1800 ppm)
600 at Nicaragua and drop off towards Costa Rica and Guatemala (≤ 500 ppm); in
601 contrast to H₂O contents, CO₂ contents do not vary systematically with
602 geochemical slab signatures such as Ba/La (Wehrmann et al. 2011). Felsic
603 melt inclusions have CO₂ concentrations below detection limits. CO₂/K₂O
604 values are much higher for Nicaragua than for other parts of the volcanic front
605 (Fig. 6b). This is certainly partly due to the K-poor nature of primitive melt
606 inclusions there, as discussed above for H₂O. In contrast to H₂O, which in
607 Nicaragua reaches only 1.4 times the maximum concentrations of adjacent
608 regions, the highest CO₂ contents of mafic melt inclusions in Nicaragua are 3
609 times those in the other parts of the arc such that relatively higher CO₂/K₂O
610 than H₂O/K₂O values are to be expected. On the other hand, most of the K-
611 poor, more MORB-like samples (cf. Sadofsky et al. 2008) come from the
612 Nejapa and Granada volcanic systems, which contribute little to the overall
613 magma and K₂O fluxes of the east-Nicaraguan arc segment (cf. Walker et al.
614 1990; Freundt et al. 2006; Avellan et al. 2012) such that using the largest
615 CO₂/K₂O values would strongly bias the volatile flux calculations for
616 Nicaragua. However, the melt inclusion data define both water-rich and water-
617 poor degassing paths in CO₂ vs. H₂O space which indicate that all melts had
618 exsolved CO₂ at pressures ≤ 500 MPa prior to melt-inclusion entrapment, with
619 more extensive exsolution for melt compositions with high slab contributions
620 (Wehrmann et al. 2011). Thus all measured CO₂ contents yield minimum
621 estimates of magmatic CO₂ flux. As a conservative estimate we calculate the
622 arc CO₂ fluxes using the envelope of CO₂/K₂O values indicated in Fig. 6b but
623 emphasize that uncertainties remain particularly large for CO₂.

624

625 Chlorine

626 Chlorine contents in felsic rocks are higher than in mafic rocks, and maximum
627 chlorine contents in the felsic rocks decrease northward probably as an effect
628 of increasing apatite fractionation associated with the change from dacite to
629 rhyolite as the most evolved composition. Cl/K₂O ratios decrease from
630 maximum values at Nicaragua towards Costa Rica and Guatemala in both
631 mafic and evolved volcanic rocks, and we use a parameterization of along-arc
632 variation as shown in Fig. 6c to estimate magmatic chlorine fluxes.

633

634 Sulfur

635 Sulfur contents do not show a systematic variation along the arc in mafic
636 rocks. Felsic melts are all strongly depleted in sulfur relative to mafic
637 compositions. The along-arc variation of S/K₂O in mafic-rock melt inclusions is
638 shown in Fig. 6d.

639

640 Volatile fluxes

641 Figure 7 and Table 2 summarize the along-arc variations in long-term average
642 mass fluxes (per unit arc length) of magma, K₂O and the volatile species for
643 the tectonic segments of the volcanic front. The spreadsheet provided as
644 electronic supplement is an extension of Table 2 of Kutterolf et al. (2008) that
645 includes the detailed volatile flux calculations. The largest source of error in
646 the magma fluxes (that translates into all other fluxes) are uncertainties in the
647 age of volcanoes; with a mix of well and poorly constrained ages on each
648 segment we estimate a typical error for segment-wise fluxes of ±20%.

649 Considering uncertainties in the parameterization of volatile compositions
650 (Fig. 6) the total error on volatile fluxes may be about $\pm 40\%$ (Fig. 7).
651 The unsteady but overall northward increase in magma and K_2O fluxes largely
652 controls a similar pattern in the H_2O fluxes while Cl fluxes remain roughly
653 constant along the arc. Particularly large fluxes of CO_2 and sulfur result for
654 Nicaragua. For the whole arc, the volatile fluxes from the mantle to the
655 volcanic front are 6.18 Tg/Ma/m H_2O , 0.17 Tg/Ma/m CO_2 , 0.54 Tg/Ma/m S,
656 and 0.22 Tg/Ma/m Cl. The CO_2 flux is smaller than the value of 0.67 Tg/Ma/m
657 calculated by Wehrmann et al. (2011) using the Nicaraguan maximum
658 CO_2/K_2O values for the entire volcanic front (cf. Fig. 6b). These mass fluxes
659 indicate a long-term average composition of volatiles delivered from the
660 mantle source to the arc volcanoes of 87% H_2O , 2.5% CO_2 , 7.5% S and 3%
661 Cl (ignoring other volatile species). Compared to the average subduction input
662 composition, the average output composition has almost the same
663 proportions of H_2O and Cl but is depleted in CO_2 and enriched in S.
664
665 At surface pressure conditions, the solubilities of H_2O , CO_2 and S in silicate
666 melt are very small (e.g., Blank et al. 1993; Behrens et al. 2004; Botcharnikov
667 et al. 2004; Carroll 2005; Dixon et al. 1995; King and Holloway 2002; Papale
668 1999) such that the fluxes of these volatiles into the atmosphere can be
669 assumed equal to their fluxes into the volcanoes, although a minor fraction
670 may remain stored in the crust (in hydrous minerals, crustal fluids). However,
671 this is not true for chlorine because, on average, about half the initial Cl
672 content is retained in the matrix glasses of the volcanic rocks.
673

674 5.2. Present-day gas fluxes

675 Another approach to assess mass fluxes at the volcanic arc makes use of the
676 monitored degassing of SO₂ at active volcanoes. We have compiled data from
677 optical remote sensing of gas plumes at 17 Central American volcanoes
678 (others are not monitored or not presently degassing) that was obtained
679 during the last 25 years (Mather et al. 2006; Hilton et al. 2002; Zimmer et al.
680 2004; Andres and Kasgnoc 1998) and own unpublished data obtained in the
681 SFB574 and NOVAC (Network for Observation of Volcanic and Atmospheric
682 Change) projects (Frische et al. 2006; Galle et al. 2012; Bo Galle, pers.
683 comm. 2012). The measured SO₂ fluxes range from 15 to 1540 tons per day
684 (averages of the temporally varying monitoring data for each volcano). Adding
685 up available average fluxes of the volcanoes, the resulting sulfur fluxes per
686 unit arc length for each arc segment are of comparable magnitude to those
687 determined from magma masses (Fig. 8a), although they are derived from
688 only 17 compared to 71 volcanoes (note that no SO₂ flux data are available
689 for the east-Guatemalan and central-Salvadorian segments). In fact, when
690 summing up for the entire volcanic front, the present-day open-vent sulfur flux
691 from the 17 volcanoes (0.84 Tg/Ma/m) is 1.4 times larger than the sulfur flux
692 derived from the long-term magma fluxes at the 71 volcanoes; it is also larger
693 than previously published open-vent flux values (≤ 0.66 Tg/Ma/m; see Fig. 12
694 below). We note that monitoring open-vent degassing may only capture part
695 of the total degassing; Shinohara (2013) found that diffuse soil and spring
696 degassing in Japan accounts for 16% of total S output (and for 39% H₂O,
697 44% CO₂, 58% Cl).

698 The magma mass fluxes required to feed the observed open-vent SO₂ fluxes
699 can be calculated using typical mafic-melt sulfur concentrations (Sadofsky et
700 al. 2008; Wehrmann et al. 2011), and are compared with the long-term
701 erupted magma fluxes for those volcanoes in Fig. 8b. The magma fluxes differ
702 by less than a factor of ten for 11 out of the 17 volcanoes. The major reason
703 why mass-flux estimates from the two approaches differ significantly is
704 probably their greatly differing time scales of observation (10¹ versus 10⁵
705 years), because both volcanic magma emission rates and open-vent
706 degassing rates vary over wide ranges of time scales. Another difference is
707 that quiescent degassing may derive from magmas that never erupt whereas
708 the long-term approach based on erupted magma masses does not capture
709 intrusive magmas that never made it to the surface. The "intrusive"
710 component of arc magmatism certainly remains the major factor of uncertainty
711 in the estimation of magma and volatile mass fluxes.

712

713 5.3. Arc output versus subduction input

714 Here we focus on the arc output versus trench input comparison because fluid
715 emissions through the forearc are comparatively very small (chapter 4). For
716 water and chlorine the outputs at the arc account for about <26% and <20%
717 of the respective inputs at the trench. The relative output of CO₂ (0.1-2.3%) is
718 an order of magnitude lower compared to H₂O and Cl except at Nicaragua
719 where it reaches 5% (Fig. 9). On the other hand, the relative sulfur outputs
720 derived from both long-term magma fluxes (9-82%) and present-day open-
721 vent monitoring (3-197%) significantly exceed the relative outputs of the other
722 volatiles (Fig. 9). Recycling efficiencies determined by Ruscitto et al. (2012)

723 using magma fluxes of Sadofsky et al. (2008) and input fluxes including
724 mantle serpentinization of van Keken et al. (2011) are similar to our values for
725 H₂O, Cl and S but about 10 times larger for CO₂ (Fig. 9). We will later discuss
726 the significance of the different input-output relationships but at this point the
727 comparison serves to emphasize the imbalance between input and output
728 volatile fluxes. Since the output at the arc only accounts for a minor fraction of
729 the input particularly for H₂O - which is the dominant volatile component by
730 mass - we clearly need to look for other sinks in the subduction system.

731

732 **6. Other volatile reservoirs in the subduction system**

733 In the following we review information on additional volatile reservoirs in the
734 subduction system. We focus on Costa Rica and Nicaragua where the most
735 detailed geophysical studies of subduction zone structure are available.

736

737 6.1. Upper-plate geophysical anomalies

738 Seismic tomography has identified strongly reduced V_p , and increased V_p/V_s ,
739 in the mantle below the arc down to the subducting slab at Nicaragua; this
740 anomaly (A4 in Fig. 10) is strongest below the Concepción-Maderas
741 volcanoes but diminishes through northern to central Costa Rica (Dinc et al.
742 2011, 2010). It is plausible to assume that this anomaly reflects fluids and
743 melts in the subarc mantle, and its southward diminishing qualitatively
744 correlates with magma production rates decreasing from Nicaragua to Costa
745 Rica (Fig. 7), decreasing geochemical slab signals (e.g., Ba/La) in arc-magma
746 compositions (Carr et al. 1990), and a change from extensional to
747 compressional tectonic stresses (Walther et al. 2000; Marshall and Anderson

748 1995; La Femina et al. 2009). Only in the lower half of the subarc anomaly at
749 Nicaragua (approximately from 200 to 100 km depth, about 50 km cross-arc
750 width) do mantle temperatures exceed the wet peridotite solidus (e.g.,
751 Peacock et al. 2005; Rüpke et al. 2002) such that volatiles may be withdrawn
752 via ascending melts. Elsewhere in the anomaly volatiles are trapped in
753 hydrous minerals formed in the mantle.

754 Another seismic velocity anomaly lies in the upper-plate lithosphere, where it
755 extends from the contact to the subducting slab at 30-50 km depth towards
756 the Nicaraguan volcanic arc (A1 to A2 in Fig. 10; Dinc et al. 2011). This is
757 interpreted as a sub-forearc hydrated zone that accumulates fluid that is
758 released from the slab at greater depths and migrates upward along the
759 steeply (c.80°) dipping slab. The further transport of fluids from near the slab
760 toward the arc is probably facilitated by extensional faulting (Dinc et al. 2011).
761 However, the discovery of northwestward trench-parallel flow in the mantle
762 wedge (Hoernle et al. 2008; Rabbel et al. 2011) also suggests a lateral
763 component of volatile transport that may add to the observed reservoirs.

764

765 The strongest negative velocity anomaly at Costa Rica comprises the forearc
766 to about 20 km depth (A5 in Fig. 10), probably reflecting strong hydration
767 facilitated by intense fracturing of the forearc by seamount subduction (Arroyo
768 et al. this volume; Dinc et al. 2010). A seismic velocity anomaly at the tip of
769 the mantle wedge (A6 in Fig. 10) is also observed at central Costa Rica but is
770 less well developed compared to Nicaragua. This anomaly has been
771 interpreted to result either from hydration of the mantle tip (Dinc et al. 2010) or
772 from underplating by eroded forearc material (Arroyo et al. 2009; this volume).

773 No such anomaly at the mantle wedge has been detected at northern Costa
774 Rica (DeShon et al. 2006; Dinc et al. 2010) suggesting limited or absent
775 mantle-wedge hydration. Below the volcanic arc of Costa Rica there is only a
776 very small negative velocity anomaly in the uppermost crust (A7 in Fig. 10).
777

778 A magnetotelluric profile across northern Costa Rica basically supports the
779 seismic anomalies there as zones of high electrical conductivity due to
780 hydration (Brasse et al., 2009; Worzewski et al. 2011). By reviewing global
781 magnetotelluric subduction zone data, Worzewski et al. (2011) concluded that
782 a hydrated region (their low-resistivity anomaly G, projected as A3 into Fig.
783 10) at 20-40 km depth and 20-40 km in front of the volcanic arc exists in many
784 mature subduction zones around the globe.
785

786 The geophysically observed anomalies are snapshots of present conditions;
787 they cannot reveal volatile fluxes but they can be interpreted in terms of
788 stored water masses. These can be determined by measuring the volume per
789 unit arc length enclosed by the ΔV_p isolines, and estimate water contents in
790 the anomaly volumes from the simple relation
791

792 $H_2O \text{ (wt\%)} = -0.31 * \Delta V_p(\%)$
793

794 (Carlson and Miller 2003) ignoring P-T dependencies that are insignificant
795 compared to other uncertainties. Here we obtain minimum estimates for the
796 stored water masses by just considering the $\Delta V_p = -4\%$ volumes with the water
797 concentration corresponding to that value (i.e., ignoring lower water contents

798 outside and higher water contents inside these volumes). In order to
799 understand the instantaneous distribution of water in the subduction system,
800 we also calculate the mass of water (per unit arc length) introduced into the
801 system during the time the slab takes to descend from the trench to sub-arc
802 depth (229 Tg/m at Nicaragua, 103 Tg/m at Costa Rica), to then determine
803 the fractions of the total water stored in each reservoir.

804 The amount of water stored in the Nicaraguan sub-arc anomaly A4 (2000
805 km³/km volume per unit arc length, 74.4 Tg/m) then would correspond to 21
806 wt% of the total water in the subduction system. The large anomaly A1 to A2
807 (1400 km³/km, 52.1 Tg/m) would account for another 15 wt% of water. The
808 water content in the low-resistivity anomaly G (A3 in Fig. 10) as determined by
809 Worzewski et al. (2011) would be barely 1 wt% of the total, hence an
810 insignificant fraction compared to A1-A2 with which it overlaps. At Costa Rica,
811 no significant hydration below the arc has yet been detected, partly due to
812 insufficient spread of seismic profiles across the arc. The anomaly A6 at the
813 tip of the mantle wedge is small (150-375 km³/km; Dinc et al. 2010; Arroyo et
814 al. this volume), making up 1-5 wt% of the total water. We do not include the
815 large Costa Rican forearc anomaly A5 (Dinc et al. 2010) in this budget
816 because this is probably mostly fed by expelled pore water rather than
817 mineral-bound water.

818 In summary, reservoirs outside the subducting slab hold between 12 wt% (at
819 Costa Rica) and 35 wt% (at Nicaragua) of the total water presently stored in
820 the subduction system. We do not know, however, if these reservoirs are in a
821 transient state, shrinking or swelling, or in a steady state where water influx
822 and outflux are balanced.

823

824 6.2. Volatile fluxes beyond subarc depths

825 Numerical modeling based on experimental investigations of the metamorphic
826 dehydration of subducting slabs predicts that the cooler (i.e., older and faster-
827 sinking) the slab the larger the fraction of water that is retained in the slab to
828 beyond sub-arc depths (Schmidt and Poli 2003; Rüpke et al. 2004; Hacker
829 2008). Also, cooler slabs are expected to store more water initially particularly
830 in serpentinized uppermost mantle (Iyer et al. 2012) such that absolute and
831 relative fluxes of water into the deep mantle increase with slab age. For
832 Central America with slab ages of 15-20 Ma, Rüpke et al. (2004) predicted
833 that <10% of the initial water content are retained beyond sub-arc depths
834 mainly by the serpentinized slab mantle. Recent modeling by van Keken et al.
835 (2011) applied to Central America, which considers three scenarios of no,
836 20% or full serpentinization of uppermost slab mantle, shows that water flux
837 with the slab decays to <60% of the input at 150 km depth, and <30% at 230
838 km depth. Sub-arc depths to the slab top range from 78-106 km at Guatemala
839 through 118-148 km at Nicaragua to 80-120 km at Costa Rica (Syracuse and
840 Abers 2006), and fluid released between 150-230 km may flow updip into the
841 sub-arc region (cf. Tsuno et al. 2012) so that it is difficult to define the depth
842 where flux into deep mantle may be determined. Faccenda et al. (2012)
843 identified a stress-controlled process of fluid transport in the slab even without
844 involving high-pressure hydrous minerals, and they conclude from their model
845 that water transfer into deep mantle remains <20% of the input. Global
846 modeling over geologic time scales constrained by sea-level changes
847 suggests that about 40% of subducted water reach the deeper mantle (Parai

848 and Mukhopadhyay 2012). In summary, a minimum of 20-30% of water input
849 into the Central American subduction system may be lost to mantle reflux.

850

851 7. Discussion

852 7.1. Comparing input fluxes

853 Almost all studies investigating subduction zone volatile input have focussed
854 on water, and some have considered only selected lithologies of the
855 downgoing slab. Figure 11 compares results for total slab H₂O input either for
856 Central America or globally, where global data have been recalculated to
857 44,000 km total subduction zone length. Obviously input fluxes based on
858 sediment and crust compositions alone are lower than those which also
859 consider serpentinized mantle. Where serpentinized mantle is included in the
860 budget, flux estimates vary widely due to large uncertainties in the extent of
861 serpentinization (cf. Rüpke et al. 2002, 2004, and van Keken et al. 2011). Our
862 results for Central America make use of the latest geophysical observations
863 that now include both across- and along-trench profiling but focus on Costa
864 Rica and Nicaragua such that much greater uncertainty remains for El
865 Salvador and Guatemala. Apart from our study here, only Hacker (2008)
866 explicitly included the effect of subduction erosion on the water input.
867 Compared to the more recently estimated global average input fluxes of water
868 (Rüpke et al. 2004; Hacker 2008; van Keken et al. 2011; Parai and
869 Mukhopadhyay 2012) our estimates for Central America are about two times
870 higher (Fig. 11) confirming earlier observations that the subducting Cocos
871 plate is unusually wet largely due to mantle serpentinization (e.g., Abers et al.
872 2003). Lateral variations in input flux along the 1265 km long Middle America

873 trench, as well as those along the 1480 km long Chile trench (Völker et al.,
874 this volume), are wider than the ranges of individual global estimates.
875
876 Subduction fluxes of other volatiles than water have been rarely investigated.
877 Previously estimated global average input fluxes of CO₂ are 5 Tg/Ma/m
878 (Peacock 1990), 5-23 Tg/Ma/m (Bebout 1996) and 3.4 Tg/Ma/m (Jarrard
879 2003). Jarrard's value for Central America of 8.6 Tg/Ma/m is similar to our
880 average value of 9.3 Tg/Ma/m (where the range over subduction segments is
881 7.8-11.4 Tg/Ma/m) while Li and Bebout (2005) calculated a lower value of 5.7
882 Tg/Ma/m CO₂. The chlorine input fluxes determined by Jarrard (2003) of 0.47
883 Tg/Ma/m (average global input) and 0.66 Tg/Ma/m (Central America), and by
884 Straub and Layne (2003) for the Izu subduction zone of 0.1 Tg/Ma/m, are
885 significantly lower than our average value of 1.62 Tg/Ma/m Cl (range 1.27-
886 1.85 Tg/Ma/m). Alt et al. (2013) estimate a global average sulfur subduction
887 rate of ~1.8 Tg/Ma/m similar to our 1.6 Tg/Ma/m for Central America.

888

889 7.2. Comparing arc output fluxes

890 The range of water output fluxes along the Central American volcanic arc
891 (CAVA) is almost as wide as the range of previously estimated arc water
892 fluxes (Fig. 12). Only Carmichael's (2002) water fluxes based on the Crisp
893 (1984) arc volcanic plus plutonic magma fluxes are significantly higher. Water
894 fluxes of the Chilean Southern Volcanic Zone are typically lower than at
895 Central America except for one segment between the Valdivia and Chiloé
896 fracture zones (Völker et al. 2011, this volume). We have also included in Fig.
897 12 the modeled water flux released from the slab to 150 km depth according

898 to van Keken et al. (2011) for the cases of no serpentinization, 20%
899 serpentinization and full serpentinization of the uppermost 2 km of slab
900 mantle. The seismological studies discussed in section 3.3 suggest that the
901 depth of serpentinization offshore Nicaragua is probably greater than in the
902 20%/2 km assumption of van Keken et al. and their corresponding H₂O input
903 flux of 28 Tg/Ma/m is only half our value of 62 Tg/Ma/m for Nicaragua, which
904 is actually similar to their input flux for full serpentinization (60 Tg/Ma/m). We
905 therefore think that van Keken et al. underestimated the depth of
906 serpentinization and, as a compromise, their modeled release flux of water
907 from the slab for the full-serpentinization scenario may be compared to our
908 arc output fluxes. This water-release flux of about 24 Tg/Ma/m is significantly
909 larger than the output fluxes of 6-8 Tg/Ma/m that we calculate for the
910 Nicaraguan arc segments. Since slab-derived water is also distributed into
911 upper-plate reservoirs apart from the arc (see section 6.1), modeling results
912 and our observation-based calculations do at least qualitatively agree.

913

914 Our CO₂ flux from the CAVA, which is based on melt-inclusion analyses, is
915 considerably lower than fluxes derived from hydrothermal and gas emissions
916 (Fig. 12). In order to obtain similar fluxes with our method, we would have
917 needed, for example, to assume melt CO₂/K₂O ≥ 1 along the entire arc (cf. Fig.
918 6b). This underlines that the petrological method strongly underestimates
919 poorly soluble magmatic volatiles such as CO₂.

920 However, this may not necessarily be true for sulfur, because our
921 petrologically estimated sulfur fluxes of the CAVA straddle the upper limit of
922 published fluxes derived from open-vent degassing (Fig. 12). On the other

923 hand, our review of recent open-vent degassing rates yields a still much
924 higher arc sulfur flux and suggests that previous calculations based on less
925 abundant monitoring data have underestimated true fluxes. Most segments of
926 the Chilean Southern Volcanic Zone yield sulfur fluxes much less than at
927 Central America except for the segment between the Valdivia and Chiloè
928 fracture zones (Völker et al. this volume).

929 As for H₂O, our chlorine emission fluxes along the CAVA largely cover the
930 range of previously estimated fluxes (Fig. 12). On average the CAVA chlorine
931 fluxes are somewhat higher than at the Southern Volcanic Zone in Chile but
932 the along-arc variation is larger there.

933

934 7.3. Output vs. input: sources and sinks of volatiles

935

936 Water

937 Figure 9 compares the outputs at the arc to the inputs at the trench; we
938 neglect here the emissions at the forearc because they are minor for water
939 and we assume that they are also minor for Cl and S. While there are along-
940 arc variations, on average the water output at the arc accounts for roughly
941 10% of the water input at the trench. This is similar to 13% estimated by
942 Straub and Layne (2003) for Izu arc and 4-8% for Chile (Völker et al., this
943 volume); Jarrard's (2003) calculations yield much higher 27-81%, Parai and
944 Mukhopadhyay (2012) modeled 53%, and Wallace (2005) concluded that
945 input and output fluxes of water are roughly balanced but Jarrard and Wallace
946 both did not consider water input by serpentinized mantle.

947 Our arc magma fluxes include an "intrusive" component insofar as we have
948 also considered the masses of primitive magma required to generate the
949 masses of evolved magma that had actually erupted (cf. Kutterolf et al. 2008).
950 We now extend that approach by also considering a "plutonic component" that
951 never forms a trace at the surface. Using plate-kinematic constraints, Phipps
952 Morgan et al. (2008) argued that an intrusion rate of 90-180 km³/Ma/km would
953 be required to half or fully balance crustal extension at the arc. Clift and
954 Vannucchi (2004) calculated intrusion rates around 100 km³/Ma/km to allow
955 for crustal growth in the presence of subduction erosion. Thus total magma
956 intrusion into the arc crust may be as large as 234-468 Tg/Ma/m (cf. Fig. 7)
957 such that our volcanic mean-CAVA magma flux of 106 Tg/Ma/m would
958 account for 45-23 wt% of total arc magma production. We note with caution,
959 however, that the rate of crustal growth is averaged over a time frame of
960 1.5x10⁷ years compared to the ~10⁵ years time window of our magma flux
961 estimates. Moreover, intrusion rates may have varied laterally along the arc.
962 Hence, the ratio between "volcanic" and "plutonic" rates may vary temporally
963 and spatially but here we assume a constant ratio. In addition, we make the
964 assumption that the hidden plutonic magmas followed the same along-arc
965 compositional variations that we derived from the volcanic rocks (Fig. 6). Then
966 the volatile output/input percentages (Fig. 9, Table 2) would have to be
967 approximately multiplied by a factor of 2-5 and the segment-wise variation of
968 relative water output would range from 9-98% with a mean CAVA value of
969 about 40%. Allowing 20-30% of the input to be carried to beyond sub-arc
970 depths (see section 6.2), we still have 40-30% not accounted for. In section
971 6.1 we have estimated that the upper-plate low-velocity anomalies hold 12%

972 (Costa Rica) to 35% (Nicaragua) of the present instantaneous distribution of
973 water in the subduction system. Thus, if we assume the highest
974 plutonic/volcanic ratio for Nicaragua where there is the greatest crustal
975 extension (Phipps Morgan et al. 2008), we achieve an almost closed water
976 budget: 40% transfer from mantle to arc, 20% in subarc velocity anomaly A4,
977 15% in anomaly A1 to A2, A3 (Fig. 10), and 20-30% into the deeper mantle
978 seem to satisfy a closed budget. For Costa Rica, however, even allowing
979 generous 30% transfer to the arc and 12% into the "seismic anomalies", we
980 fail to account for more than half the input. The slab crust as the main carrier
981 of water (Fig. 4) is thicker than at Nicaragua to Guatemala, and additional
982 igneous ocean-crust material is subducted by forearc erosion. Particularly the
983 gabbroic crust may keep its water to beyond sub-arc depths (van Keken et al.
984 2011). We speculate that the relative water flux into the deep mantle is larger
985 at Costa Rica than farther north and may account for about (or more than?)
986 half the input flux.

987

988 Probably most magmatic water reaching the arc is derived from the subducted
989 slab because primitive melt H₂O contents correlate positively with
990 geochemical slab signatures (e.g., Ba/La; Sadofsky et al. 2008; Ruscitto et al.
991 2012) and magmatic H₂O/K₂O ratios distinctly exceed those of both N- and E-
992 MORB type mantle (Fig. 6a; Michael 1988). A source distribution such as in
993 the global modeling of Parai and Mukhopadhyay (2012), with only 3% of the
994 water emitted at the volcanic arcs originally stemming from the mantle wedge
995 but 97% being derived from the subducting slabs, probably also applies to the
996 Central American subduction system.

997

998 Carbon dioxide

999 The volcanic CO₂ output determined by our petrologic method is typically <2%
1000 of the input but reaches 5% at Nicaragua. Both closed- and open-system
1001 CO₂-degassing was common in these magmas (Wehrmann et al. 2011) such
1002 that CO₂ contents are petrologically underestimated. Arc CO₂ outputs derived
1003 from hydrothermal and gas emissions are higher (Fig. 12) but still only
1004 account for 6-24% of the input. He-CO₂ and δ¹³C relationships of Central
1005 American hydrothermal and gas emissions indicate that the provenance of
1006 CO₂ released along the volcanic front is dominated by subducted marine
1007 carbonates (L=76±4%) and organic sediments (S=14±3%), with the mantle
1008 wedge (M) contributing only 10±3% to the total carbon flux (Shaw et al. 2003;
1009 de Leeuw et al. 2007). These geochemical observations seem to contradict
1010 petrological studies implying that carbonate phases are stable to beyond
1011 subarc depths in limestone (Kerrick and Connolly 2001), serpentized mantle
1012 (Kerrick and Connolly 1998) and carbonated ocean crust (Molina and Poli
1013 2000), and released fluids are very CO₂-poor (except for unusual high-T low-P
1014 conditions). This apparent contradiction may be resolved in two ways:
1015 (1) Aqueous fluids from the lower lithological units of the slab may react with
1016 carbonate in the metasediment layer if percolation is pervasive rather than
1017 channeled to produce a CO₂-rich fluid entering the mantle wedge (Kerrick and
1018 Connolly 2001; Schmidt and Poli 2003). Gorman et al. (2006) modelled CO₂
1019 release from the sediment and upper crust of the slab by either channelized
1020 or pervasive flow of fluid from underlying lithologies for the Nicaraguan
1021 subduction conditions. The CO₂ flux from the slab is about an order of

1022 magnitude greater for pervasive than channelized flow, but for both CO₂
1023 liberation occurs at sub-forearc rather than subarc depths. Carbonate veins in
1024 subduction-zone metamorphosed rocks are quite common, demonstrating
1025 mobilization of C (e.g., Cartwright and Barnicoat 1999; Sadofsky and Bebout
1026 2004), and C-O isotopic compositions of these veins indicate a slab derivation
1027 of C from both inorganic marine/hydrothermal and organic sources (van der
1028 Straaten et al. 2012). Thus, while veins have been abundantly observed in
1029 high-pressure metamorphic rocks (e.g., John et al. 2008; Gao et al. 2007; van
1030 der Straaten et al. 2012), geochemistry of the hydrothermal and gas
1031 emissions seems to suggest that pervasive flow is required to liberate
1032 substantial amounts of carbon from the source lithologies.

1033 (2) An alternative explanation of sub-arc CO₂ transfer makes use of the
1034 modeled ascent of metasediment diapirs at temperatures of 500-850°C that
1035 serves to introduce fluid-insoluble slab elements into the mantle wedge (Behn
1036 et al. 2011). Tsuno et al. (2012) show experimentally that near-solidus melting
1037 of Al-poor carbonated pelite at P≥5 GPa produces alkali-rich carbonatite melt.
1038 They propose that immiscible carbonatite melt formed at 220-250 km depth
1039 rises updip to sub-arc depth and then via metasediment diapirs into the
1040 mantle wedge. This model can explain both geochemical signals (e.g. high
1041 Ba/La) and high CO₂ flux at Nicaragua.

1042

1043 Chlorine

1044 The close similarity between chlorine and water in terms of input and output
1045 flux variations along the subduction zone, relative importance of input
1046 lithologies, and input-output flux ratio (Figs. 3, 4, 7, 9) suggests that both

1047 volatiles may behave similarly during the various metamorphic and magmatic
1048 processes. Scambelluri et al. (2004) showed that Cl contents decrease
1049 strongly from oceanic serpentinites to high-pressure serpentinites and
1050 anhydrous olivine-orthopyroxene rocks representative of prograde slab
1051 metamorphism of ultramafic rocks and conclude that Cl quantitatively enters
1052 the slab-derived fluid. Kendrick et al. (2012), on the other hand, argue that
1053 serpentinite retains a significant fraction of Cl beyond sub-arc depths. Still
1054 most of the Cl contained in the arc-volcanic rocks would be derived from the
1055 slab. Cl/K₂O values of the volcanic melt inclusions (Fig. 6c) are significantly
1056 higher than in N- or E-MORB type mantle (e.g., Kent et al. 2002) and are
1057 largest at Nicaragua where other geochemical signatures suggest maximum
1058 slab contribution (e.g., Carr et al. 1990). In contrast, Barnes et al. (2009)
1059 interpreted chlorine isotope compositions of Central American arc rocks to
1060 support a slab-source dominance only at Nicaragua while favoring a mantle-
1061 source dominance for Costa Rica and El Salvador/Guatemala. However, later
1062 work (John et al. 2010) showed that the chlorine isotope compositional range
1063 of subducted sediment is wider than previously thought such that it overlaps
1064 completely with the arc rock compositions. Noting wide ranges of Cl/H₂O in
1065 arc magmatic compositions, Wallace (2005) argued that Cl and H₂O become
1066 strongly fractionated while processed through the subduction zone. The
1067 observation by Straub and Layne (2003) that Izu-arc Cl output makes good for
1068 77% of the input, but water only for 13%, seems to support such fractionation
1069 but they did not consider slab mantle serpentinitization in their budget. Our
1070 observation that the relative outputs of Cl and H₂O are roughly correlated
1071 need not contradict Cl-H₂O fractionation at the local process scale but

1072 suggests that over larger spatial and time scales such fractionations balance
1073 out to some correlated behavior.
1074
1075 Sulfur
1076 The output-input ratio for sulfur is much larger than for the other volatiles, a
1077 result shown by both the long-term fluxes based on melt inclusion analyses
1078 and the present-day fluxes based on open-vent monitoring (Fig. 9). The
1079 S/K₂O values of Nicaraguan melt inclusions, which have the least evolved
1080 compositions, are near the value for primitive mantle (Fig. 6d; McDonough
1081 and Sun 1995). However, S-concentrations up to 2500 ppm in Central
1082 American primitive melt inclusions (Sadofsky et al. 2008) would require about
1083 400-500 ppm S in the mantle source (cf. de Hoog et al. 2001), i.e. roughly
1084 twice the concentration of 250 ppm S expected in fertile mantle (McDonough
1085 and Sun 1995). Moreover, rocks and glasses from the Mariana and Japan
1086 arcs have elevated $\delta^{34}\text{S}$ isotope values which suggest slab-derived additions
1087 to the mantle source (Alt et al. 1993; Ueda and Sakai 1984). To our
1088 knowledge, the fate of S-bearing minerals in sediment during high-P slab
1089 metamorphism has not yet been systematically studied. Recently Jago and
1090 Dasgupta (2013) showed experimentally that partial melts of subducted
1091 MORB would be very S-poor (<50 ppm) but coexisting fluids would be very S-
1092 rich (10-15 wt%) and could remove almost half the sulfur from the slab crust.
1093 Hattori and Guillot (2007) determined ≤ 5 ppm S in Alpine and Cuban high-
1094 pressure serpentinites originally formed from abyssal peridotites, and Alt et al.
1095 (2013) conclude that significant fluid escape of sulfur is delayed until the
1096 transformation from antigorite serpentinite to chlorite harzburgite. We

1097 tentatively conclude that contributions of S from the slab are complemented
1098 by S originally hosted in the mantle wedge in order to explain why the arc
1099 output / trench input ratio is much larger for sulfur than for the other volatiles.

1100

1101 8. Conclusions

1102 We have reviewed the presently available information on the Central
1103 American subduction zone in order to constrain a budget of volatiles (H₂O,
1104 CO₂, Cl, S) carried into, processed through, and expelled out of the system.
1105 Regarding the input into the subduction zone by the downgoing slab, we have
1106 extended earlier approaches by considering mineral-bound rather than pore-
1107 water chlorine, by including sulfur in the budget, and by explicitly including
1108 volatile subduction fluxes via serpentinized slab mantle and the removal of
1109 forearc basement (typically accreted oceanic crust) by subduction erosion.
1110 While volatile input fluxes gradually increase from Guatemala to Nicaragua,
1111 there is a jump in input-flux values toward Costa Rica because of a strong
1112 change in subduction lithologies: thicker ocean crust, stronger subduction
1113 erosion but little mantle serpentinization. We find that H₂O and Cl fluxes are
1114 mainly controlled by serpentinized mantle, CO₂ fluxes by subducted sediment
1115 which includes carbonates, and S fluxes by subducted oceanic crust including
1116 accreted crust removed by subduction erosion. The range of input fluxes
1117 along the Middle America Trench covers a large part of the total range of
1118 published global volatile input-flux estimates.

1119

1120 Analyses of fluid and carbonate compositions and flux measurements at cold
1121 seeps along the Central American forearc allow to estimate that about 2 wt%

1122 of mineral-bound H₂O subducted at the trench is expelled through the forearc,
1123 probably mostly derived from subducted sediment. Mixing of seep fluids with
1124 seawater and biogenic in addition to thermogenic methane production mask
1125 any emission of other volatiles (CO₂, Cl, S) from the slab through the forearc.
1126
1127 The major output of volatiles is their transfer from the slab through the mantle
1128 wedge to the arc crust, and finally into the exosphere, by arc magmatism. We
1129 have used an extensive data set of geochemically and petrologically
1130 determined melt volatile concentrations in combination with volcanologically
1131 determined long-term (~10⁵ years) average magma fluxes which consider
1132 both proximal, edifice-forming deposits and widely dispersed tephras as well
1133 as the intrusive masses required to produce the observed evolved
1134 compositions, in order to calculate the volatile fluxes to the arc. As an
1135 alternative approach, we have also used present-day open-vent gas-flux
1136 measurements to determine sulfur and associated magma fluxes. While both
1137 approaches yield similar along-arc variations, they greatly differ in the time
1138 scales of observation of transient processes. Our volcanological and
1139 geochemical data set for Central America, which is probably one of the most
1140 detailed records worldwide, defined the along-arc variations in magma and
1141 volatile fluxes that we then extrapolated to the hidden plutonic magma flux
1142 that has been derived from crustal growth rates of the past 15 Ma (Clift and
1143 Vannucchi 2004; Phipps Morgan et al. 2008). This extrapolation led to 2-5
1144 times higher mantle-to-crust volatile fluxes compared to the purely volcanic
1145 rates.

1146 The along-arc variations of water and chlorine fluxes cover a large fraction of
1147 the range of global arc flux estimates. While our sulfur fluxes tend to be higher
1148 than published estimates, our petrological approach underestimates CO₂
1149 fluxes compared to gas and hydrothermal He-CO₂ relationships. Even though
1150 the thermal state of the Cocos slab intermediate between "hot" and "cold"
1151 extremes should provide optimum conditions for sub-arc fluid release
1152 (Ruscitto et al. 2012), the volatile (H₂O, CO₂, Cl) transfer through the arc only
1153 accounts for a fraction of the volatile input at the trench, even if we consider
1154 "invisible" intrusions as required by crustal growth. For sulfur, however, the
1155 output flux at the arc may approximately balance the input flux at the trench.
1156 Recent numerical models simulating the stability of hydrous mineral phases
1157 under the pressure-temperature conditions in slab lithologies subducting at
1158 Central America found that 20-30% of the water input may be transferred
1159 beyond subarc depths into the deeper mantle (Rüpke et al. 2004; van Keken
1160 et al 2011). Such mantle reflux plus the mantle-wedge to arc flux still leaves a
1161 deficiency of 30-40% of the input. We conclude that at least some of this
1162 deficiency corresponds to the water stored in upper-plate regions identified as
1163 anomalies of low seismic velocities and/or electrical resistivities: a lithospheric
1164 to asthenospheric subarc region widely enveloping melt ascent pathways, and
1165 a lithospheric region extending from the slab below the forearc to below the
1166 arc. We have estimated the present, static distribution of water into these
1167 anomalies but do not know if they are temporally variable. However, the fact
1168 that the static distribution is very similar to the flux distribution expected from
1169 the overall water budget, we suspect that these water reservoirs may be in a
1170 near-steady state where input and output fluxes are roughly balanced.

1171

1172 Acknowledgements

1173 We thank David Pyle and an anonymous reviewer, as well as Erwin Suess as

1174 topic editor, for critical comments that greatly helped to improve this paper.

1175 This publication is contribution no. 261 of the Sonderforschungsbereich 574

1176 “Volatiles and Fluids in Subduction Zones” at Kiel University.

1177

1178 References

1179 (* marks SFB 574 contributions)

1180 Abers GA, Plank T, Hacker BR (2003) The wet Nicaraguan slab. *Geophys Res Lett* 30: 1098,

1181 doi:10.1029/2002GL015649

1182 Alt JC (1994) A sulfur isotopic profile through the Troodos ophiolite, Cyprus: Primary

1183 composition and the effects of seawater hydrothermal alteration. *Geochim Cosmochim*

1184 *Acta* 58: 1825-1840

1185 Alt JC, Schwarzenbach EM, Früh-Green GL, Shanks WC, Bernasconi SM, Garrido CJ,

1186 Crispini L, Gaggero L, Padron-Navarta JA, Marchesi C (2013) The role of serpentinites

1187 in cycling of carbon and sulfur: Seafloor serpentinitization and subduction

1188 metamorphism. *Lithos* 178: 40-54

1189 Alt JC, Shanks WC (1998) Sulfur in serpentinitized oceanic peridotites: Serpentinization

1190 processes and microbial sulfate reduction. *J Geophys Res* 103: 9917-9929

1191 Alt JC, Shanks WC (2003) Serpentinization of abyssal peridotites from the MARK area, Mid-

1192 Atlantic Ridge: Sulfur geochemistry and reaction modeling. *Geochim Cosmochim Acta*

1193 67: 641-653

1194 Alt JC, Shanks WC (2006) Stable isotope compositions of serpentinite seamounts in the

1195 Mariana forearc: Serpentinization processes, fluid sources and sulfur metasomatism.

1196 *Earth Planet Sci Lett* 242: 272-285

- 1197** Alt JC, Shanks WC, Jackson MC (1993) Cycling of sulfur in subduction zones: the
1198 geochemistry of sulfur in the Mariana Arc and back-arc trough. *Earth Planet Sci Lett*
1199 119: 477-494
- 1200** Andres RJ, Kasgnoc AD (1998) A time-averaged inventory of subaerial volcanic sulphur
1201 emissions. *J Geophys Res* 103: 25,251–25,651
- 1202** * Arroyo IG, Husen S, Flueh E, Gossler J, Kissling E, Alvarado GE (2009) Three-dimensional
1203 P-wave velocity structure on the shallow part of the Central Costa Rican Pacific margin
1204 from Local Earthquake Tomography using off- and onshore networks. *Geophys J Int*,
1205 doi: 10.1111/j.1365-246X.2009.04342.x
- 1206** * Arroyo IG, Husen S, Flüh ER (2013) The seismogenic zone in the Central Costa Rican
1207 Pacific margin: high-quality hypocenters from an amphibious network. *Int J Earth Sci*,
1208 this volume DOI 10.1007/s00531-013-0955-8
- 1209** Avellan DR, Macias JL, Pardo N, Scolamacchia T, Rodriguez D (2012) Stratigraphy,
1210 geomorphology, geochemistry and hazard implications of the Nejapa Volcanic Field,
1211 western Managua, Nicaragua. *J Volcanol Geotherm Res* 213-214: 51-71,
1212 doi:10.1016/j.jvolgeores.2011.11.002
- 1213** Azema J, Bourgois J, Baumgartner PO, Tournon J, Desmet A, Auboin J (1982) A tectonic
1214 cross-section of the Costa Rican Pacific littoral as a key to the structure of the landward
1215 slope of the Middle America trench off Guatemala. *Init Rep DSDP* 84: 831-850
- 1216** Bach W, Rosner M, Jöns N, Rausch S, Robinson LF, Paulick H, Erzinger J (2011) Carbonate
1217 veins trace seawater circulation during exhumation and uplift of mantle rock: Results
1218 from ODP Leg 209. *Earth Planet Sci Lett* 311: 242-252
- 1219** Barnes JD, Sharp ZD (2006) A chlorine isotope study of DSDP/ODP serpentinitized ultramafic
1220 rocks: insights into the serpentinitization process. *Chem Geol* 228: 246–265
- 1221** Barnes JD, Sharp ZD, Fischer TP, Hilton DR, Carr MJ (2009) Chlorine isotope variations
1222 along the Central American volcanic front and back arc. *Geochem Geophys Geosys*
1223 10: Q11S17, doi:10.1029/2009GC002587
- 1224** Bebout GE (1996) Volatile Transfer and Recycling at Convergent Margins: Mass-Balance and
1225 Insights from High-P/T Metamorphic Rocks (Overview). In: GE Bebout, DW Scholl, SH

- 1226** Kirby, JP Platt (eds) Subduction – Top to bottom, AGU Geophysical Monograph 96:
1227 179-193
- 1228** Bebout GE, Bebout AE, Graham CM (2007) Cycling of B, Li, and LILE (K, Cs, Rb, Ba, Sr) into
1229 subduction zones: SIMS evidence from micas in high-P/T metasedimentary rocks.
1230 Chem Geol 239: 284-304
- 1231** Behn MD, Kelemen PB, Hirth G, Hacker BR, Massonne HJ (2011) Diapirs as the source of
1232 the sediment signature in arc lavas. Nature Geoscience 4: 641-646
- 1233** Behrens H, Ohlhorst S, Holtz F, Champenois M (2004) CO₂ solubility in dacitic melts
1234 equilibrated with H₂O-CO₂ fluids: Implications for modeling the solubility of CO₂ in silicic
1235 melts. Geochim Cosmochim Acta 68: 4687-4703
- 1236** Blank JG, Stolper EM, Carroll MR (1993) Solubilities of carbon dioxide and water in rhyolitic
1237 melt at 850°C and 750 bars. Earth Planet Sci Lett 119:27-36
- 1238** Bonifacie M, Jendrzewski N, Agrinier P, Coleman M, Pineau F, Javoy M (2007)
1239 Pyrohydrolysis-IRMS determination of silicate chlorine stable isotope compositions.
1240 Application to oceanic crust and meteorite samples. Chem Geol 242: 187-201
- 1241** Botcharnikov RE, Behrens H, Holtz F, Koepke J, Sato H (2004) Sulfur and chlorine solubility
1242 in Mt. Unzen rhyodacite melt at 850°C and 200 MPa. Chem Geol 213: 207-225
- 1243** * Brasse H, Kapinos G, Mütschard L, Alvarado GE, Worzewski T, Jegen M (2009) Deep
1244 electrical resistivity structure of northwestern Costa Rica. Geophys Res Lett 36:
1245 L02310, doi:10.1029/2008GL036397
- 1246** Carlson RL, Miller DJ (2003) Mantle wedge water contents estimated from seismic velocities
1247 in partially serpentinized peridotites. Geophys Res Lett 30: 1250,
1248 doi:10.1029/2002GL016600
- 1249** Carmichael ISE (2002) The andesite aqueduct: perspectives on the evolution of intermediate
1250 magmatism in west-central (105-99°W) Mexico. Contrib Mineral Petrol 143: 641-663
- 1251** Carr MJ (1984) Symmetrical and segmented variation of physical and geochemical
1252 characteristics of the Central American volcanic front. J Volcanol Geotherm Res 20:
1253 231-252

- 1254** Carr MJ, Feigenson MD, Bennett EA (1990) Incompatible element and isotopic evidence for
1255 tectonic control of source mixing and melt extraction along the central American arc.
1256 Contrib Mineral Petrol 105: 369-380
- 1257** Carr MJ, Feigenson MD, Patino LC, Walker JA (2003) Volcanism and geochemistry in Central
1258 America: Progress and problems. In: Eiler JM (ed) Inside the subduction factory. AGU
1259 Geophysical Monograph Series 138: 153-179
- 1260** Carr MJ, Patino LC, Feigenson MD (2007) Petrology and geochemistry of lavas. In:
1261 Buntschuh J, Alvarado GE (eds) Central America – Geology, resources and hazards.
1262 Balkema, Rotterdam, vol. 1: 565-590
- 1263** Carroll MR (2005) Chlorine solubility in evolved alkaline magmas. Ann Geophys 48: 619-631
- 1264** Cartwright I, Barnicoat AC (1999) Stable isotope geochemistry of Alpine ophiolites: a window
1265 to ocean-floor hydrothermal alteration and constraints on fluid–rock interaction during
1266 high-pressure metamorphism. Int J Earth Sci 88: 219–235
- 1267** Christeson GL, McIntosh KD, Shipley TH, Flueh ER, Goedde H (1999) Structure of the Costa
1268 Rica convergent margin, offshore Nicoya Peninsula. J Geophys Res 104: 25,443–
1269 25,468
- 1270** Clift P, Vannucchi P (2004) Controls on tectonic accretion versus erosion in subduction
1271 zones: Implications for the origin and recycling of the continental crust. Rev Geophys
1272 42: doi:10.1029/2003RG000127
- 1273** Crisp JA (1984) Rates of magma emplacement and volcanic output. J Volcanol Geotherm
1274 Res 20: 177-211
- 1275** De Hoog JCM, Mason PRD, Van Bergen MJ (2001) Sulfur and chalcophile elements in
1276 subduction zones: Constraints from laser-ablation ICP-MS study of melt inclusions from
1277 Galunggung volcano, Indonesia. Geochim Cosmochim Acta 65: 3147-3164
- 1278** De Leeuw GAM, Hilton DR, Fischer TP, Walker JA (2007) The He–CO₂ isotope and relative
1279 abundance characteristics of geothermal fluids in El Salvador and Honduras: New
1280 constraints on volatile mass balance of the Central American Volcanic Arc. Earth
1281 Planet Sci Lett 258: 132-146

- 1282** Delacour A, Früh-Green GL, Bernasconi SM, Schaeffer P, Kelley DS (2008a) Carbon
1283 geochemistry of serpentinites in the Lost City Hydrothermal System (30°N, MAR).
1284 *Geochim Cosmochim Acta* 72: 3681-3702
- 1285** Delacour A, Früh-Green GL, Bernasconi SM (2008b) Sulfur mineralogy and geochemistry of
1286 serpentinites and gabbros of the Atlantis Massif (IODP Site U1309). *Geochim*
1287 *Cosmochim Acta* 72: 5111-5127
- 1288** Delmelle P, Stix J, Baxter PJ, Garcia-Alvarez J, Barquero J (2002) Atmospheric dispersion,
1289 environmental effects and potential health hazard associated with the low-altitude gas
1290 plume of Masaya volcano, Nicaragua. *Bull Volcanol* 64: 423-434
- 1291** DeMets C (2001) A new estimate for present-day Cocos-Caribbean plate motion: Implications
1292 for slip along the Central American volcanic arc. *Geophys Res Lett* 28: 4043-4046
- 1293** DePaolo DJ (1983) The mean life of continents: estimates of continental recycling rates from
1294 Nd and Hf isotopic data and implications for mantle structure. *Geophys Res Lett* 10:
1295 705–708
- 1296** * DeShon HR, Schwartz SY, Newman AV, González V, Protti M, Dorman LM, Dixon TH,
1297 Sampson DE, Flueh ER (2006) Seismogenic zone structure beneath the Nicoya
1298 Peninsula, Costa Rica, from three-dimensional local earthquake P- and S-wave
1299 tomography. *Geophys J Int* 164: 109-124, doi: 10.1111/j.1365-246X.2005.02809.x
- 1300** * Dinc AN, Koulakov I, Thorwart M, Rabbel W, Flüh ER, Arroyo I, Taylor W, Alvarado G
1301 (2010) Local Earthquake Tomography of Central Costa Rica: Transition from seamount
1302 to ridge subduction. *Geophys J Int* 183: 286-302, doi: 10.1111/j.1365-
1303 246X.2010.04717.x
- 1304** * Dinc AN, Rabbel W, Flüh ER, Taylor W (2011) Mantle wedge hydration in Nicaragua from
1305 local earthquake tomography. *Geophys J Int* 186: 99-112, doi: 10.1111/j.1365-
1306 246X.2011.05041.x
- 1307** Dixon JE, Stolper EM, Holloway JR (1995) An experimental study of water and carbon dioxide
1308 solubilities in mid-ocean ridge basaltic liquids. Part I: Calibration and solubility models.
1309 *J Petrol* 36: 1607-1631

- 1310** Domanik KJ, Holloway R (1996) Stability and composition of phengitic muscovite and
1311 associated phases from 5.5 to 11 GPa: Implications for deeply subducted sediments.
1312 *Geochim Cosmochim Acta* 60: 4133-4150
- 1313** Ehrenborg J (1996) A new stratigraphy for the Tertiary volcanic rocks of the Nicaraguan
1314 highland. *Geol Soc Am Bull* 108: 830-842
- 1315** Eickmann B, Bach W, Peckmann J (2009) Geochemical constraints on the modes of
1316 carbonate precipitation in peridotites from the Logatchev Hydrothermal Vent Field and
1317 Gakkel Ridge. *Chem Geol* 268: 97–106
- 1318** Faccenda M, Gerya TV, Mancktelow NS, Moresi L (2012) Fluid flow during slab unbending
1319 and dehydration: Implications for intermediate-depth seismicity, slab weakening and
1320 deep water recycling. *Geochem Geophys Geosyst* 13: Q01010,
1321 doi:10.1029/2011GC003860
- 1322** Feigenson MD, Carr MJ, Maharaj SV, Juliano S, Bolge LL (2004) Lead isotope composition of
1323 Central American volcanoes: Influence of the Galapagos plume. *Geochemistry,*
1324 *Geophysics, Geosystems* 5: Q06001, doi:10.1029/2003GC000621
- 1325** Fischer TP (2008) Fluxes of volatiles (H₂O, CO₂, N₂, Cl, F) from arc volcanoes. *Geochem J*
1326 42: 21-38
- 1327** * Freundt A, Kutterolf S, Schmincke HU, Hansteen TH, Wehrmann H, Perez W, Strauch W,
1328 Navarro M (2006) Volcanic hazards in Nicaragua: Past, present, and future. In: Rose
1329 WI, Bluth G, Carr MJ, Ewert J, Patino L, Vallance J (eds) *Volcanic hazards in Central*
1330 *America*. *Geol Soc Am Spec Paper* 412: 141-165, doi: 10.1130/2006.2412(08)
- 1331** * Frische M, Garofalo K, Hansteen TH, Borchers R (2006) Fluxes and origin of halogenated
1332 organic trace gases from Momotombo volcano (Nicaragua). *Geochem Geophys*
1333 *Geosyst* 7: Q05020, doi:10.1029/2005GC001162
- 1334** Galle B, Arellano S, Norman P, Conde V, and the NOVAC Team (2012) Inventory of gas flux
1335 measurements from volcanoes of the global Network for Observation of Volcanic and
1336 Atmospheric Change (NOVAC). *Geophys Res Abs* 14, EGU2012-8988-2, EGU
1337 General Assembly 2012

- 1338** * Gao J, John T, Klemd R, Xiong X (2007) Mobilisation of Ti-Nb-Ta during subduction:
1339 Evidence from rutile-bearing dehydration segregations and veins hosted in eclogite,
1340 Tianshan, NW China. *Geochim Cosmochim Acta* 71: 4974-4996,
1341 doi:10.1016/j.gca.2007.07.027
- 1342** Gerya T (2011) Future directions in subduction modeling. *J Geodyn* 52: 344-378
- 1343** Gerya TV, Meilick FI (2010) Geodynamic regimes of subduction under an active margin:
1344 effects of rheological weakening by fluids and melts. *J metam Geol* 29: 7-31
- 1345** Gorman PJ, Kerrick DM, Connolly JAD (2006) Modeling open system metamorphic
1346 decarbonation of subducting slabs. *Geochem Geophys Geosyst* 7: Q04007,
1347 doi:10.1029/2005GC001125
- 1348** * Grevemeyer I, Kaul N, Diaz-Naveas JL, Villinger HW, Ranero CR, Reichert C (2005) Heat
1349 flow and bending-related faulting at subduction trenches: Case studies offshore of
1350 Nicaragua and Central Chile. *Earth Planet Sci Lett* 236: 238-248
- 1351** * Grevemeyer I, Ranero CR, Flüh ER, Kläschen D, Bialas J (2007) Passive and active
1352 seismological study of bending-related faulting and mantle serpentinization at the
1353 Middle America trench. *Earth Planet Sci Lett* 258: 528-542
- 1354** Hacker BR (2008) H₂O subduction beyond arcs. *Geochem Geophys Geosys* 9: Q03001,
1355 doi:10.1029/2007GC001707
- 1356** * Halama R, Bebout GE, John T, Scambelluri M (2012) Nitrogen recycling in subducted
1357 mantle rocks and implications for the global nitrogen cycle. *Int J Earth Sci* (this volume)
1358 DOI 10.1007/s00531-012-0782-3
- 1359** * Han X, Suess E, Sahling H, Wallmann K (2004) Fluid venting activity on the Costa Rica
1360 margin: New results from authigenic carbonates. *Intl J Earth Sci (Geol Rdsch)* 93: 596-
1361 611
- 1362** * Hansen KW, Wallmann K (2003) Cretaceous and cenozoic evolution of seawater
1363 composition, atmospheric O₂ and CO₂: a model perspective. *Am J Sci* 303: 94-148
- 1364** Hattori KH, Guillot S (2007) Geochemical character of serpentinites associated with high- to
1365 ultrahigh-pressure metamorphic rocks in the Alps, Cuba, and the Himalayas: Recycling

- 1366** of elements in subduction zones. *Geochem Geophys Geosyst* 8: Q09010,
1367 doi:10.1029/2007GC001594
- 1368** * Hensen C, Wallmann K (2005) Methane formation at Costa Rica continental margin –
1369 constraints for gas hydrate inventories and cross-décollement fluid flow. *Earth Planet*
1370 *Sci Lett* 236: 41-60
- 1371** * Hensen C, Wallmann K, Schmidt M, Ranero CR, Suess E (2004) Fluid expulsion related to
1372 mud extrusion off Costa Rica - a window to the subducting slab. *Geology* 32: 201-204
- 1373** Hilton DR, Fischer TP, Marty B (2002) Noble gases and volatile recycling at subduction
1374 zones. *Rev Miner* 47: 319–370
- 1375** Hoernle K, van den Bogaard P, Werner R, Lissinna B, Hauff F, Alvarado G, Garbe-Schönberg
1376 D (2002) Missing history (16-71 Ma) of the Galápagos hotspot: Implications for the
1377 tectonic and biological evolution of the Americas. *Geology* 30: 795-798
- 1378** * Hoernle K, Abt DL, Fischer KM, Nichols H, Hauff F, Abers G, van den Bogaard P, Heydolph
1379 K, Alvarado G, Protti JM, Strauch W (2008) Arc-Parallel Flow in the Mantle Wedge
1380 Beneath Costa Rica and Nicaragua. *Nature*, doi: 10.1038/nature06550
- 1381** Ito E, Harris DM, Anderson AT (1983) Alteration of oceanic crust and geologic cycling of
1382 chlorine and water. *Geochim Cosmochim Acta* 47: 1613-1624
- 1383** * Ivandic M, Grevemeyer I, Berhorst A, Flueh E. R, McIntosh K. (2008). Impact of bending
1384 related faulting on the seismic properties of the incoming oceanic plate offshore of
1385 Nicaragua. *J Geophys Res* 113: B05410, doi:10.1029/2007JB005291
- 1386** * Ivandic M, Grevemeyer I, Bialas J, Petersen CJ (2010) Serpentinization in the trench-outer
1387 rise region offshore of Nicaragua: constraints from seismic refraction and wide-angle
1388 data. *Geophys J Int* 180: 1253-1264
- 1389** Iyer K, Rüpke LH, Grevemeyer I, Phipps Morgan J (2012) Controls of faulting and reaction
1390 kinetics on serpentinization and double Benioff zones. *Geochem Geophys Geosyst* 13:
1391 Q09010, doi:10.1029/2012gc004304
- 1392** Jarrard RD (2003) Subduction fluxes of water, carbon dioxide, chlorine, and potassium.
1393 *Geochem Geophys Geosyst* 4: 8905, doi: 10.1029/2002GC000392

- 1394** Jégo S, Dasgupta R (2013) Fluid-present melting of sulfide-bearing ocean crust: Experimental
1395 constraints on the transport of sulfur from slab to mantle wedge. *Geochim Cosmochim*
1396 *Acta* 110: 106-134, doi: 10.1016/j.gca.2013.02.011
- 1397** * John T, Klemd R, Gao J, Garbe-Schönberg CD (2008) Trace-element mobilization in slabs
1398 due to non steady-state fluid-rock interaction: constraints from an eclogite-facies
1399 transport vein in blueschist (Tianshan, China). *Lithos*, 103: 1-24, doi:
1400 10.1016/j.lithos.2007.09.005
- 1401** * John T, Layne GD, Haase KM, Barnes JD (2010) Chlorine isotope evidence for crustal
1402 recycling into the Earth's mantle. *Earth Planet Sci Lett* 298: 175-182, DOI:
1403 10.1016/j.epsl.2010.07.039
- 1404** * John T, Scambelluri M, Frische M, Barnes J D, Bach W (2011) Dehydration of subducting
1405 serpentinite: implications for halogen mobility in subduction zones and the deep
1406 halogen cycle. *Earth Planet Sci Lett* 308: 65-76, doi:10.1016/j.epsl.2011.05.038
- 1407** * Karaca D, Hensen C, Wallmann K (2010) Controls on authigenic carbonate precipitation at
1408 cold seeps along the convergent margin off Costa Rica. *Geochem. Geophys. Geosyst.*
1409 11: Q08S27, doi:10.1029/2010GC003062
- 1410** * Karaca D, Schleicher T, Hensen C, Linke P, Wallmann K (2012) Quantification of methane
1411 emission from bacterial mat sites at Quepos Slide offshore Costa Rica. *Int J Earth Sci*
1412 (this volume) DOI 10.1007/s00531-012-0839-3
- 1413** Kendrick MA, Honda M, Pettke T, Scambelluri M, Phillips D, Giuliani A (2013) Subduction
1414 zone fluxes of halogens and noble gases in seafloor and forearc serpentinites. *Earth*
1415 *Planet Sci Lett* 365: 86-96
- 1416** Kendrick MA, Woodhead JD, Kamenetsky VS (2012) Tracking halogens through the
1417 subduction cycle. *Geology* 40: 1075-1078
- 1418** Kent AJR, Peate DW, Newman S, Stolper EM, Pearce JA (2002) Chlorine in submarine
1419 glasses from the Lau Basin: seawater contamination and constraints on the
1420 composition of slab-derived fluids. *Earth Planet Sci Lett* 202: 361-377
- 1421** Kerrick DM, Connolly JAD (1998) Subduction of ophiocarbonates and recycling of CO₂ and
1422 H₂O. *Geology* 26: 375-378

- 1423** Kerrick DM, Connolly JAD (2001) Metamorphic devolatilization of subducted marine
1424 sediments and the transport of volatiles into the Earth's mantle. *Nature* 411: 293-296
- 1425** Kim JJ, Matumoto T, Latham GV (1982) A crustal section of northern Central America as
1426 inferred from wide-angle reflections from shallow earthquakes. *Bull seism Soc Am* 72:
1427 925-940
- 1428** Kimura G, Silver EA, Blum P, et al. (1997) Site 1039. *Proc ODP Init Repts* 170: 45-93
- 1429** King PL, Holloway JR (2002) CO₂ solubility and speciation in intermediate (andesitic) melts:
1430 The role of H₂O and composition. *Geochim Cosmochim Acta* 66: 1627-1640
- 1431** * Kutterolf S, Freundt A, Pérez W (2008) The Pacific offshore record of Plinian arc volcanism
1432 in Central America, part 2: Tephra volumes and erupted masses. *Geochem Geophys*
1433 *Geosys* 9, doi:10.1029/2007GC001791
- 1434** * Kutterolf S, Hansteen TH, Appel K, Freundt A, Krüger K, Perez W, Wehrmann H (2013)
1435 Combined bromine and chlorine release from large explosive volcanic eruptions: A
1436 threat to stratospheric ozone? *Geology*, doi:10.1130/G34044.1
- 1437** La Femina P, Dixon TH, Govers R, Norabuena E, Turner H, Saballos A, Mattioli G, Protti M,
1438 Strauch W (2009), Fore-arc motion and Cocos Ridge collision in Central America.
1439 *Geochem Geophys Geosyst* 10: Q05S14, doi:10.1029/2008GC002181
- 1440** Lange RA, Frey HM, Hector J (2009) A thermodynamic model for the plagioclase-liquid
1441 hygrometer/thermometer. *Am Mineral* 94: 494-506
- 1442** * Lefeldt M, Grevemeyer I (2008) Centroid depth and mechanism of trench-outer rise
1443 earthquakes. *Geophys J Int* 172: 240-251, doi: 10.1111/j.1365-246X.2007.03616
- 1444** * Lefeldt M, Grevemeyer I, Gossler J, Bialas J (2009) Intraplate seismicity and related mantle
1445 hydration at the Nicaraguan trench outer rise. *Geophys J Int* 178: 742-752,
1446 doi:10.1111/j.1365-246X.2009.04167.x
- 1447** * Lefeldt M, Ranero CR, Grevemeyer I (2012) Seismic evidence of tectonic control on the
1448 depth of water influx into incoming oceanic plates at subduction trenches. *Geochem*
1449 *Geophys Geosyst* 13: Q05013, doi:10.1029/2012GC004043

- 1450** Li L, Bebout GE (2005) Carbon and nitrogen geochemistry of sediments in the Central
1451 American convergent margin: Insights regarding subduction input fluxes, diagenesis,
1452 and paleoproductivity. *J Geophys Res* 110: B11202, doi:10.1029/2004JB003276
- 1453** * Liebetrau V, Augustin N, Kutterolf S, Schmidt M, Eisenhauer A, Garbe-Schönberg D,
1454 Weinrebe W (2014) Authigenic carbonate archives of mound and slide related fluid
1455 venting at the Central American Forearc: Geochemical and mineralogical insights. *Int J*
1456 *Earth Sci* (this volume)
- 1457** * Linke P, Wallmann K, Suess E, Hensen C, Rehder G (2005) In-situ benthic fluxes from an
1458 intermittently active mud volcano at the Costa Rica convergent margin. *Earth Planet*
1459 *Sci Lett* 235: 79-95, doi: 10.1016/j.epsl.2005.03.009
- 1460** * Lu Z, Hensen C, Fehn U, Wallmann K (2007) Old iodine in fluids venting along the Central
1461 American convergent margin. *Geophys Res Lett*: L22604, doi:10.1029/2007/GL031864
- 1462** * Lücke O (2012) Moho structure of Central America based on three-dimensional lithospheric
1463 density modelling of satellite derived gravity data. *Int J Earth Sci* (this volume) DOI
1464 10.1007/s00531-012-0787-y
- 1465** MacKenzie L, Abers GA, Fisher KM, Syracuse EM, Protti JM, Gonzales V, Strauch W (2008)
1466 Crustal structure along the southern Central American volcanic front. *Geochem*
1467 *Geophys Geosyst* 9/8: Q08S09, doi:10.1029/2008GC001991
- 1468** Mann P, Rogers RD, Gahagan L (2007) Overview of plate tectonic history and its unresolved
1469 tectonic problems. In: Buntschuh J, Alvarado GE (eds) *Central America – Geology,*
1470 *resources and hazards*. Balkema, Rotterdam, 205-241
- 1471** Marshall JS, Anderson RS (1995) Quaternary uplift and seismic cycle deformation, Peninsula
1472 de Nicoya, Costa Rica. *Bull Geol Soc Am* 107: 463–473
- 1473** Marty B, Tolstikhin IN (1998) CO₂ fluxes from mid-ocean ridges, arcs and plumes. *Chem Geol*
1474 145: 233-248
- 1475** Mather TA, Pyle DM, Tsanev VI, McGonigle AJS, Oppenheimer C, Allen AG (2006) A
1476 reassessment of current volcanic emissions from the Central American arc with specific
1477 examples from Nicaragua. *J Volcanol Geotherm Res* 149: 297-311

- 1478** * Mau S, Sahling H, Rehder G, Suess E, Linke P, Soeding E (2006) Estimates of methane
1479 output from mud extrusions at the erosive convergent margin off Costa Rica. *Marine*
1480 *Geology* 225: 129-144
- 1481** * Mau S, Rehder G, Arroyo IG, Gossler J, Suess E (2007) Indications of a link between
1482 seismotectonics and CH₄ release from seeps off Costa Rica. *Geochem Geophys*
1483 *Geosys* 8, Q04003, doi:10.1029/2006GC001326
- 1484** * Mau S, Rehder G, Sahling H, Schleicher T, Linke P (2012) Seepage of methane at Jaco
1485 Scar, a slide caused by seamount subduction offshore Costa Rica. *Int J Earth Sci*: DOI
1486 10.1007/s00531-012-0822-z (this volume)
- 1487** * Mavromatis V, Botz R, Schmidt M, Liebetrau V, Hensen C (2012) Formation of carbonate
1488 concretions in surface sediments of two mud mounds offshore Costa Rica: A stable
1489 isotope study. *Int J Earth Sci* (this volume) DOI 10.1007/s00531-012-0843-7
- 1490** McDonough WF, Sun SS (1995) The composition of the Earth. *Chem Geol* 120: 223-253
- 1491** * Metzner D, Toohey M, Kutterolf S, Freundt A, Niemeier U, Timmreck C, Krüger K (2012)
1492 Radiative forcing and climate impact resulting from the SO₂ injections based on a
1493 200,000 year record of Plinian eruptions along the Central American Volcanic Arc. *Int J*
1494 *Earth Sci*, DOI 10.1007/s00531-012-0814-z (this volume)
- 1495** Michael PJ (1988) The concentration, behaviour and storage of H₂O in the suboceanic upper
1496 mantle: implications for mantle metasomatism. *Geochim Cosmochim Acta* 52: 555-566
- 1497** Molina JF, Poli S (2000) Carbonate stability and fluid composition in subducted oceanic crust:
1498 an experimental study on H₂O-CO₂-bearing basalts. *Earth Planet Sci Lett* 176: 295-310
- 1499** Moore GF, Saffer D, Studer M, Costa Pisani P (2011) Structural restoration of thrusts at the
1500 toe of the Nankai Trough accretionary prism off Shikoku Island, Japan: Implications for
1501 dewatering processes. *Geochem Geophys Geosyst* 12: Q0AD12,
1502 doi:10.1029/2010GC003453
- 1503** * Mörz T, Fekete N, Kopf A, Brückmann W, Kreiter S, Hünerbach V, Masson DG, Hepp DA,
1504 Schmidt M, Kutterolf S, Sahling H, Abegg F, Spieß V, Suess E, Ranero CR, (2005)
1505 Styles and productivity of mud diapirism along the Middle American margin, part II:
1506 Mound Culebra and Mounds 11, and 12. In Martinelli G, Panahi B (eds) *Mud*

- 1507** volcanoes, geodynamics and seismicity. NATO Sci. Ser. IV: Dordrecht (Springer): 49-
1508 76
- 1509** Papale P (1999) Modeling of the solubility of a two-component H₂O+CO₂ fluid in silicate
1510 liquids. Am Mineral 84: 477-492
- 1511** Parai R, Mukhopadhyay S (2012) How large is the subducted water flux? New constraints on
1512 mantle regassing rates. Earth Planet Sci Lett 317-318: 396-406
- 1513** Patino LC, Carr MJ, Feigenson MD (2000) Local and regional variations in Central American
1514 arc lavas controlled by variations in subducted sediment input. Contrib Mineral Petrol
1515 138: 265-283
- 1516** Peacock SM (1990) Fluid processes in subduction zones. Science 248: 329-337
- 1517** Peacock SM (2001) Are the lower planes of double seismic zones caused by serpentine
1518 dehydration in subducting oceanic mantle? Geology 29: 299-302
- 1519** Peacock SM, van Keken PE, Holloway SD, Hacker BR, Abers GA, Ferguson RL (2005)
1520 Thermal structure of the Costa Rica – Nicaragua subduction zone. Phys Earth Planet
1521 Int 149: 187-200
- 1522** * Phipps-Morgan J, Ranero CR, Vannucchi P (2008) Intra-arc extension in Central America:
1523 Links between plate motions, tectonics, volcanism, and geochemistry. Earth Planet Sci
1524 Lett 272: 365-371, doi: 10.1016/j.epsl.2008.05.004
- 1525** Plank T, Langmuir CH (1998) The chemical composition of subducting sediment and its
1526 consequences for the crust and mantle. Chem Geol 145: 325-394
- 1527** Puchelt H, Pritchard HM, Berner Z, Maynard J (1996) Sulfide mineralogy, sulfur content, and
1528 sulfur isotope composition of mafic and ultramafic rocks from Leg 147. Proc ODP Sci
1529 Res 147: 91-101
- 1530** Putirka KD (2008) Thermometers and barometers for volcanic systems. In: Putirka KD,
1531 Tepley FJ III (eds) Minerals, inclusions and volcanic processes, Rev Mineral Geochem
1532 69: 61-120
- 1533** Pyle DM, Mather TA (2009) Halogens in igneous processes and their fluxes to the
1534 atmosphere and oceans from volcanic activity: A review. Chem Geol 263: 110-121

- 1535** * Rabbal W, Koulatov I, Dinc AN, Jakovlev A (2011) Arc parallel shear deformation and
1536 escape flow in the mantle wedge of the Central America subduction zone: Evidence
1537 from P-wave anisotropy. *Geochem Geophys Geosyst* 12: Q05S31, doi:
1538 10.1029/2010GC003325
- 1539** Ranero CR, von Huene R (2000) Subduction erosion along the Middle America convergent
1540 margin. *Nature* 404: 748-752
- 1541** * Ranero CR, Weinrebe W (2005) Tectonic processes during convergence of lithospheric
1542 plates at subduction zones. In: Wille PC (ed) *Sound images of the Ocean*, Springer
1543 Publishing Company: 85-105
- 1544** * Ranero CR; von Huene R, Weinrebe W, Barckhausen U (2007) Convergent margin
1545 tectonics of Middle America: A marine perspective. In: Bundschuh J, Alvarado G (eds)
1546 *Central America - Geology, Hazards and Resources*. Balkema, Lisse, Niederlande,
1547 Tokio, Japan: pp. 239-265
- 1548** * Ranero CR, Grevemeyer I, Sahling H, Barckhausen U, Hensen C, Wallmann K, Weinrebe
1549 W, Vannucchi P, von Huene R, McIntosh K (2007) The hydrogeological system of
1550 erosional convergent margins and its influence on tectonics and interplate
1551 seismogenesis. *Geochem Geophys Geosys* 9: Q03S04, doi:10.1029/2007GC001679
- 1552** Ranero CR, von Huene R, Flueh E, Duarte M, Baca D, McIntosh K (2000) A cross section of
1553 the convergent Pacific margin of Nicaragua. *Tectonics* 19: 335-357
- 1554** * Ranero CR, Phipps-Morgan J, McIntosh K, Reichert C (2003) Bending, faulting and mantle
1555 serpentinization at the Middle America Trench. *Nature* 425: 367-373
- 1556** * Ranero CR, Grevemeyer I, Sahling H, Barckhausen U, Hensen C, Wallmann K, Weinrebe
1557 W, Vannucchi P, von Huene R, McIntosh K (2008) The hydrogeological system of
1558 erosional convergent margins and its influence on tectonics and interplate
1559 seismogenesis. *Geochem Geophys Geosys* 9(3): Q03S04,
1560 doi:10.1029/2007GC001679
- 1561** Ridolfi F, Renzulli A, Puerini M (2010) Stability and chemical equilibrium of amphibole in calc-
1562 alkaline magmas: an overview, new thermobarometric formulations and application to
1563 subduction-related volcanoes. *Contrib Mineral Petrol* 160: 45-66

- 1564** Robock A (2000) Volcanic eruptions and climate. *Rev Geophys* 38: 191-219
- 1565** * Rüpke LH, Phipps Morgan J, Hort M, Connolly J (2004) Serpentine and the Subduction
1566 Zone Water Cycle. *Earth Planet Sci Lett* 223: 17-34
- 1567** * Rüpke L, Phipps-Morgan J, Hort M, Connolly JAD (2002) Are the regional variations in
1568 Central American arc lavas due to differing basaltic versus peridotitic slab sources of
1569 fluids? *Geology* 30: 1035-1038
- 1570** Ruscitto DM, Wallace PJ, Cooper LB, Plank T (2012) Global Variations in H₂O/Ce: 2.
1571 Relationships to arc magma geochemistry and volatile fluxes. *Geochem Geophys*
1572 *Geosyst* 13: Q03025, doi:10.1029/2011GC003887
- 1573** * Sadofsky SJ, Bebout GE (2004) Field and isotopic evidence for fluid mobility in the
1574 Franciscan Complex: forearc paleohydrogeology to depths of 30 kilometers. *Int Geol*
1575 *Rev* 46: 1053–1088
- 1576** * Sadofsky S, Portnyagin M, Hoernle K, van den Bogaard P (2008) Subduction cycling of
1577 volatiles and trace elements through the Central American volcanic arc: evidence from
1578 melt inclusions. *Contrib Mineral Petrol* 155: 433-456, DOI:10.1007/s00410-007-0251-3
- 1579** Saffer DM (2003) Pore pressure development and progressive dewatering in underthrust
1580 sediments at the Costa Rican subduction margin: Comparison with northern Barbados
1581 and Nankai. *J Geophys Res* 108: B5, 2261, doi:10.1029/2002JB001787
- 1582** Saffer DM, Tobin HJ (2011) Hydrogeology and Mechanics of Subduction Zone Forearcs:
1583 Fluid Flow and Pore Pressure. *Annu Rev Earth Planet Sci* 39: 157-186
- 1584** * Sahling H, Masson DG, Ranero CR, Hühnerbach V, Weinrebe W, Klauke I, Bürk D,
1585 Brückmann W, Suess E (2008) Fluid seepage at the continental margin offshore Costa
1586 Rica and southern Nicaragua. *G-cubed* 9: Q05S05, doi:10.1029/2008GC001978
- 1587** Sallares V, Dañobeitia JJ, Flüh ER (2001) Lithospheric structure of the Costa Rican isthmus:
1588 Effects of subduction magmatism on an oceanic plateau. *J Geophys Res* 106: 621–
1589 643
- 1590** Sano Y, Williams SN (1996) Fluxes of mantle and subducted carbon along convergent plate
1591 boundaries. *Geophys Res Lett* 23: 2749-2752

- 1592** Scambelluri M, Münsterer O, Ottolini L, Pettke TT, Vannucci R (2004) The fate of B, Cl and Li
1593 in the subducted oceanic mantle and in the antigorite breakdown fluids. *Earth Planet*
1594 *Sci Lett* 222: 217-234
- 1595** * Schmidt M, Hensen C, Mörz T, Müller C, Grevemeyer I, Wallmann K, Mau S, Kaul N (2005)
1596 Methane hydrate accumulation in "Mound 11" mud volcano, Costa Rica forearc. *Marine*
1597 *Geology* 216: 83-100
- 1598** Schmidt MW, Poli S (1998) Experimentally based water budgets for dehydrating slabs and
1599 consequences for arc magma generation. *Earth Planet Sci Lett* 163: 361–379
- 1600** Schmidt MW, Poli S (2003) Generation of Mobile Components during Subduction of Oceanic
1601 Crust. In: Rudnick RL (ed.) *The Crust. Treatise on Geochemistry*, vol. 3, Holland HD
1602 and Turekian KK, series eds., Elsevier-Pergamon, Oxford: 567-591
- 1603** * Scholz F, Hensen, C, Schmidt M, Geersen J (2013) Submarine weathering of silicate
1604 minerals and the extent of pore water freshening at active continental margins.
1605 *Geochim Cosmochim Acta* 100: 200-216
- 1606** Shaw AM, Hilton DR, Fischer TP, Walker JA, Alvarado GE (2003) Contrasting He-C
1607 relationships in Nicaragua and Costa Rica: Insights into C cycling through subduction
1608 zones. *Earth Planet Sci Lett* 214: 499-513
- 1609** Shinohara H (2013) Volatile flux from subduction zone volcanoes: Insights from a detailed
1610 evaluation of the fluxes from volcanoes in Japan. *J Volcanol Geotherm Res* 268: 46-63
- 1611** Spinelli GA, Underwood MB (2004) Character of sediments entering the Costa Rica
1612 subduction zone: Implications for partitioning of water along the plate interface. *The*
1613 *Island Arc* 13: 432-451
- 1614** Stavenhagen AU, Flueh ER, Ranero C, McIntosh KD, Shipley T, Leandro G, Schulze A,
1615 Danobeitia JJ (1998) Seismic wide-angle investigations in Costa Rica—A crustal
1616 velocity model from the Pacific to the Caribbean coast. *Zbl Geol Palaeont H.* 3 –6: 393–
1617 408
- 1618** Straub SM, Layne GD (2003) The systematics of chlorine, fluorine, and water in Izu arc front
1619 volcanic rocks: Implications for volatile recycling in subduction zones. *Geochim*
1620 *Cosmochim Acta* 67: 4179-4203

- 1621** * Suess E (2014) Marine cold seeps and their products: manifestations of material transport,
1622 environmental conditions and tectonic settings. *Int J Earth Sci* (this volume)
- 1623** Syracuse EM, Abers GA (2006) Global compilation of variations in slab depth beneath arc
1624 volcanoes and implications. *Geochem Geophys Geosyst* 7:
1625 doi:10.1029/2005GC001045
- 1626** * Thorwart M, Dzierma Y, Rabbel W, Hensen C (2013) Seismic swarms, fluid flow and
1627 hydraulic conductivity in the forearc offshore North Costa Rica and Nicaragua. *Int J*
1628 *Earth Sci* (this volume) DOI 10.1007/s00531-013-0960-y
- 1629** Tsuno K, Dasgupta R, Danielson L, Richter K (2012) Flux of carbonate melt from deeply
1630 subducted pelitic sediments: Geophysical and geochemical implications for the source
1631 of Central American volcanic arc. *Geophys Res Lett* 39: L16307,
1632 doi:10.1029/2012GL052606
- 1633** Ueda A, Sakai H (1984) Sulfur isotope study of Quaternary volcanic rocks from the Japanese
1634 Islands Arc. *Geochim Cosmochim Acta* 48: 1837-1848
- 1635** Van Avendonk HJA, Holbrook WS, Lizarralde D, Denyer P (2011) Structure and
1636 serpentinization of the subducting Cocos plate offshore Nicaragua and Costa Rica.
1637 *Geochem Geophys Geosyst* 12: Q06009, doi:10.1029/2011GC003592
- 1638** * Van der Straaten F, Halama R, John T, Schenk V, Hauff F, Andersen N (2012) Tracing the
1639 effects of high-pressure metasomatic fluids and seawater alteration in blueschist-facies
1640 overprinted eclogites: Implications for subduction channel processes. *Chem Geol* 292-
1641 293: 69-87, doi:10.1016/j.chemgeo.2011.11.008
- 1642** Van Keken PE, Hacker BR, Syracuse EM, Abers GA (2011) Subduction factory: 4. Depth-
1643 dependent flux of H₂O from subducting slabs worldwide. *J Geophys Res* 116: B01401,
1644 doi:10.1029/2010JB007922
- 1645** * Vannucchi P, Galeotti S, Clift PD, Ranero CR, von Huene R (2004) Long-term subduction-
1646 erosion along the Guatemalan margin of the Middle America Trench. *Geology* 32: 617-
1647 620
- 1648** Vannucchi P, Scholl DW, Meschede M, McDougall-Reid K (2001) Tectonic erosion and
1649 consequent collapse of the Pacific margin of Costa Rica: Combined implications from

- 1650** ODP Leg 170, seismic offshore data, and regional geology of the Nicoya Peninsula.
- 1651** Tectonics 20: 649-668
- 1652** * Vannucchi P, Ranero CR, Galeotti S, Straub SM, Scholl DW, McDougall-Ried K (2003) Fast
- 1653** rates of subduction erosion along the Costa Rica Pacific margin: Implications for non-
- 1654** steady rates of crustal recycling at subduction zones. J Geophys Res 108: 2511, doi:
- 1655** 10.1029/2002/B002207
- 1656** * Völker D, Kutterolf S, Wehrmann H (2011) Comparative mass balance of volcanic edifices at
- 1657** the Southern Volcanic Zone of the Andes between 33°S and 46°S. J Volcanol
- 1658** Geotherm Res 205: 114-129
- 1659** * Völker D, Wehrmann H, Kutterolf S, Iyer K, Rabbel W, Geersen J, Hoernle K (2014)
- 1660** Constraining input and output fluxes of the southern Central Chile Subduction Zone:
- 1661** water, chlorine, sulfur. Int J Earth Sci (this volume)
- 1662** Von Glasow R, Bobrowski N, Kern C (2009) The effects of volcanic eruptions on atmospheric
- 1663** chemistry. Chem Geol 263: 131-142
- 1664** Von Huene R, Scholl DW (1991) Observations at convergent margins concerning sediment
- 1665** subduction, subduction erosion, and the growth of continental crust. Rev Geophys 29:
- 1666** 279-316
- 1667** von Huene R, Auboin J, Azema J, Blackington G, Carter JA, Coulburn WT, Cowan DS,
- 1668** Curiale JA, Dengo CA, Faas RW, Harrison W, Hesse R, Hussong DM, Laad JW,
- 1669** Muzylov N, Shiki T, Thompson PR, Westberg J (1980) Leg 67: The deep sea drilling
- 1670** project Mid-America trench transect off Guatemala. Geol Soc Am Bull 91: 421-432
- 1671** Walker JA, Carr MJ, Feigenson MD, Kalamarides RI (1990) The petrogenetic significance of
- 1672** interstratified high- and low-Ti basalts in central Nicaragua. J Petrol 31: 1141-1164
- 1673** Wallace PJ (2005) Volatiles in subduction zone magmas: concentrations and fluxes based on
- 1674** melt inclusion and volcanic gas data. J Volcanol Geotherm Res 140: 217-240
- 1675** Wallace PJ, Anderson AT (2000) Volatiles in magmas. In: Sigurdsson H, et al. (eds.)
- 1676** Encyclopedia of volcanoes. San Diego, Academic Press: 149–170

- 1677** * Walther C, Flüh ER (2002) Remnant of the ancient Farallon Plate breakup: A low-velocity
1678 body in the lower oceanic crust off Nicoya Peninsula, Costa Rica - evidence from wide-
1679 angle seismics. *Geophys Res Lett* 29: 45/1-4
- 1680** Walther CHE (2003) The crustal structure of the Cocos ridge off Costa Rica. *J Geophys Res*
1681 108: 2136, doi:10.1029/2001JB000888
- 1682** Walther CHE, Flueh ER, Ranero CR, von Huene R, Strauch W (2000) Crustal structure
1683 across the Pacific margin of Nicaragua: Evidence for ophiolitic basement and a shallow
1684 mantle sliver. *Geophys J Int* 141: 759-777
- 1685** * Wehrmann H, Hoernle K, Portnyagin M, Wiedenbeck M, Heydoph K (2011) Volcanic CO₂
1686 output at the Central American subduction zone inferred from melt inclusions in olivine
1687 crystals from mafic tephras. *Geochem Geophys Geosyst* 12: Q06003, doi:
1688 10.1029/2010GC003412
- 1689** * Weinrebe W, Flüh ER (eds) (2002) Cruise report SO163 - Subduction I, GEOMAR Report
1690 106, pp. 534
- 1691** Werner R, Hoernle K, Bogaard Pvd, Ranero C, Huene Rv, Korich D (1999) Drowned 14 -m.y.-
1692 old Galapagos archipelago off the cost of Costa Rica: implications for tectonic and
1693 evolutionary models. *Geology* 27: 499-502
- 1694** * Worzewski T, Jegen M, Kopp H, Brasse H, Taylor Castillo W (2011) Magnetotelluric image
1695 of the fluid cycle in the Costa Rican subduction zone. *Nature Geoscience* 4: 108-111,
1696 DOI 10.1038/ngeo1041
- 1697** Ye S, Bialas J, Flueh ER, Stavenhagen A, von Huene R (1996) Crustal structure of the
1698 subduction zone off Costa Rica derived from OBS refraction and wide-angle reflection
1699 seismic data. *Tectonics* 15: 1006–1021
- 1700** Zimmer MM, Fischer TP, Hilton DR, Alvarado GE, Sharp ZD, Walker JA (2004) Nitrogen
1701 systematics and gas fluxes of subduction zones: Insights from Costa Rica arc volatiles.
1702 *Geochem Geophys Geosyst* 5: Q05J11, doi:10.1029/2003GC000651
- 1703**
- 1704** **Figure captions**

1705 Fig. 1 Map of the Central American subduction zone. Bathymetry along the
1706 Middle America Trench shows traces of NW-SE striking bend-faults on the
1707 outer rise and seamounts and the Cocos Ridge offshore Costa Rica. The
1708 Central American Volcanic Arc (CAVA) is divided into 10 tectonic segments:
1709 WGS, CGS, EGS = west, central, east Guatemala segment; WSS, CSS, ESS
1710 = west, central, east Salvadorian segments; WNS, ENS = west and east
1711 Nicaragua segments; GCS= Guanacaste segment, CCS= Cordillera Central
1712 segment. Segment boundaries extended towards the trench parallel to the
1713 Cocos plate motion vector (arrow) serve to divide the trench into country-wise
1714 segments (GUA, ES, NIC, CR).
1715

1716 Fig. 2 Seismic velocity profiles along the trench - NW-SE profile drawn after
1717 Fig. 6 of van Avendonk et al. (2011) - and perpendicular to trench - SW-NE
1718 profile drawn after Fig. 4 of Ivandic et al. (2008). Red lines = MOHO; numbers
1719 give V_p [km/s]. The SW-NE profile shows how lower velocities descend below
1720 the MOHO with approach to the trench. NW-SE profile shows deeper-
1721 reaching low-velocity zones in the mantle of the Cocos plate offshore
1722 Nicaragua generated at the East Pacific Rise (EPR) compared to the plate
1723 segments offshore Costa Rica generated at Cocos-Nazca spreading center
1724 (CNS) and modified by Galapagos hotspot track.
1725

1726 Fig. 3 Mineral-bound volatile input fluxes for the four trench segments. See
1727 Table 1 for results. Gray inset graph shows along-trench variation in
1728 convergence rate V_c after Syracuse and Abers (2006) for comparison; gray
1729 dots are average values used in calculations for each segment.

1730

1731 Fig. 4 Fractions of the volatile input fluxes delivered by the various lithological
1732 units. Arrows mark published global average data for comparison: H08 =
1733 Hacker (2008), vK11 = Van Keken et al. (2011); J03 = Jarrard (2003).

1734

1735 Fig. 5 Map of the Nicaraguan and Costa Rican segment of the Central
1736 American subduction zone modified after Ranero et al. (2008). Dashed lines
1737 mark isotherms along the plate boundary. Colored dots mark cold seeps that
1738 occur at the middle slope across the region where plate boundary
1739 temperature 60-150°C. Black dots are interplate earthquakes that occur
1740 beyond the dewatering interval at temperatures >150°C.

1741

1742 Fig. 6 Along-arc variations in volatile concentrations. Data from analyzed melt
1743 inclusions, water-contents from plagioclase-melt equilibria and amphibole
1744 compositions. The parameterization functions (red lines) used in flux
1745 calculations have been determined as regression functions through the
1746 (visually selected) maximum volatile/K₂O values along the arc. Mantle data:
1747 N-MORB and E-MORB compositions in (a) from Michael (1988), in (c) from
1748 Kent et al. (2002), primitive mantle PM in (d) from McDonough and Sun
1749 (1995).

1750

1751 Fig. 7 Segment-wise along-arc variation in volcanic volatile fluxes based on
1752 long-term magma fluxes converted to K₂O fluxes that were multiplied by
1753 volatile/K₂O ratios. The sum of long-term fluxes from each volcano on a
1754 segment has been divided by segment length. Typical relative errors are

1755 estimated as $\pm 20\%$ for magma and K_2O fluxes and $\pm 40\%$ for volatile fluxes.

1756 The gray bar indicates magmatic intrusion rates according to Clift and

1757 Vannucchi (2004) and Phipps Morgan et al. (2008).

1758

1759 **Fig. 8** (a) Along-arc variations of arc-segment sulfur fluxes derived from long-

1760 term magma fluxes and from present-day open-vent monitoring. The sum of

1761 the mean open-vent degassing rates for each monitored volcano on a

1762 segment is divided by segment length. Standard deviations around the mean

1763 vary widely but $\pm 30\text{-}60\%$ may be typical. (b) Comparison of long-term magma

1764 fluxes with magma fluxes calculated from open-vent degassing rates. Young

1765 volcanoes Izalco (300 yrs.) and Cerro Negro (150 yrs.) have grown at rates

1766 well exceeding the long-term magma fluxes in their neighbourhood. Error bars

1767 illustrate the standard deviation around the mean of the open-vent

1768 measurements; in some cases the standard deviation is larger than the mean

1769 value (vertical dashed lines).

1770

1771 **Fig. 9** Arc-volcanic volatile output fluxes as percentage of the respective input

1772 fluxes at the trench for each segment along the arc. Sulfur data: $S(mi)$ from

1773 melt inclusions and long-term magma fluxes; $S(ov)$ from open-vent degassing.

1774 Color-coded bars beneath R-12 show recycling efficiencies from Ruscitto et

1775 al. (2012) for comparison. Their much higher efficiency for CO_2 reflects the

1776 large difference in volcanic CO_2 flux between Hilton et al. (2002) and our data

1777 (cf. Fig. 12).

1778

1779 Fig. 10 Schematic illustration of anomalies in seismic velocity (cf. Dinc et al.
1780 2010, 2011) and electrical resistivity (cf. Worzewski et al. 2011) at Nicaragua
1781 and Costa Rica.
1782

1783 Fig. 11 Comparison of published subduction input fluxes of mineral-bound
1784 water. Blue dots: without mantle serpentinization, green dots: with
1785 serpentinized mantle, orange dots: V-13= Völker et al. (this volume) for Chile
1786 (CL) subduction zone, red dots: this study, orange and red stars: mean values
1787 for Chile and Central America. g=global estimates (all for 44.000 km total
1788 subduction zone length). P-90= Peacock (1990); B-96= Bebout (1996); S&P-
1789 98= Schmidt and Poli (1998); R-02= Rüpke et al. (2002) for Costa Rica (CR)
1790 and Nicaragua (NI); J-03= Jarrard (2003) global (g) and Central America (CA)
1791 estimates; SL-03= Straub and Layne (2003) for Izu arc; R-04= Rüpke et al.
1792 (2004) model results for 20 Ma and 120 Ma old subducting lithosphere; H-08=
1793 Hacker (2008); vK-11= van Keken et al. (2011) for Guatemala-El Salvador
1794 (GS), Nicaragua (NI) and Costa Rica (CR) each with no mantle
1795 serpentinization (no s.), 2 wt% H₂O in topmost 2 km of mantle (2/2 s.) and full
1796 serpentinization (full s.) of topmost mantle; P&M-12= Parai and
1797 Mukhopadhyay (2012) global modeling over geologic time scales.
1798

1799 Fig. 12 Compilation of arc-volcanic volatile emissions. Carmichael (2002) (C-
1800 02) used DePaolo's (1983) crustal growth rate and 6 and 16 wt% H₂O to
1801 estimate global (g) arc water output. Applying the same approach to Crisp's
1802 (1984) (C-84) arc volcanic and plutonic magma flow rates yields much higher
1803 global estimates. C-02 CA and MX are Carmichael's fluxes for Central

1804 America and Mexico. SL-03= Straub and Layne (2003) Izu arc water and
1805 chlorine fluxes. J-03= Jarrard (2003) global H₂O, CO₂ and Cl fluxes. W-05=
1806 Wallace (2005) and I-83= Ito et al. (1983) global fluxes, V-13= Völker et al.
1807 (this volume) for Chile (7 segments of Southern Volcanic Zone). vK-11= water
1808 fluxes released from slab to 150 km depth for no or limited (20%)
1809 serpentinization (lower data) and for full serpentinization of uppermost mantle
1810 (upper data). Our data: star = mean CAVA, gray dots = arc segments. SW-
1811 96= Sano and Williams (1996), H-02= Hilton et al. (2002), S-03= Shaw et al.
1812 (2003), Z-04= Zimmer et al. (2004), M-06= Mather et al. (2006), dL-07= de
1813 Leeuw et al. (2007), F-08= Fischer (2008), PM-09= Pyle and Mather (2009),
1814 S-13= Shinohara (2013) all use hydrothermal and open-vent emissions to
1815 constrain volatile fluxes globally (g), for Central America (CA), Nicaragua (NI),
1816 Costa Rica (CR) and El Salvador (ES). For sulfur we compare our fluxes from
1817 open-vent degassing (ov) with those from melt-inclusion compositions (mi).
1818
1819 **Table 1** Properties of Cocos Plate lithological units and calculated volatile
1820 input fluxes for the four segments of the Middle America Trench (Fig. 1).
1821
1822 **Table 2** Summary of volcanic mass fluxes (per unit arc length) from the
1823 mantle wedge to the arc for the 10 arc segments. An extended version with all
1824 calculations is provided as electronic supplement.

Figure 1
[Click here to download high resolution image](#)

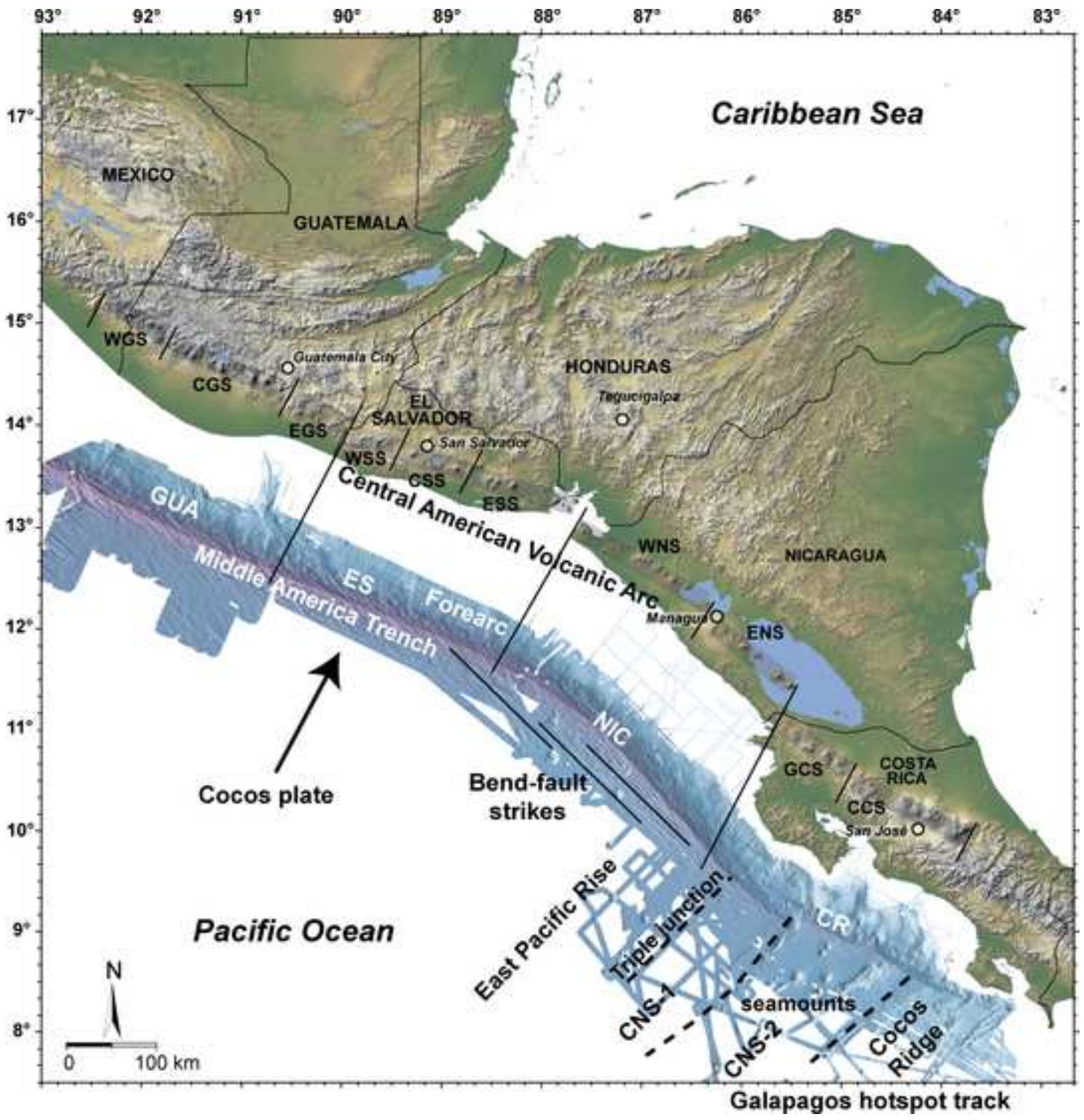


Figure 2
[Click here to download Figure: Fig2.eps](#)

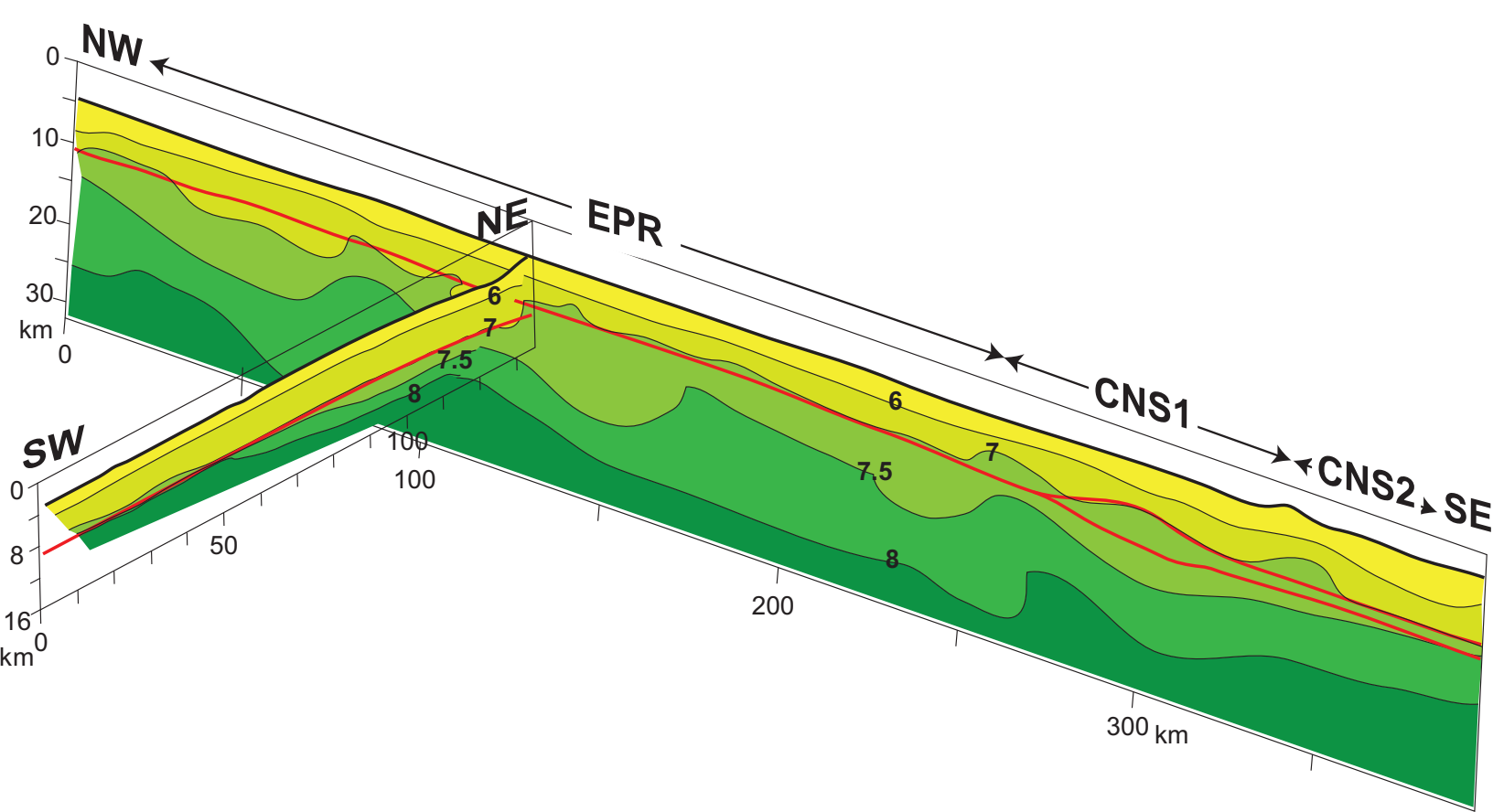


Figure 3
[Click here to download Figure: Fig3.eps](#)

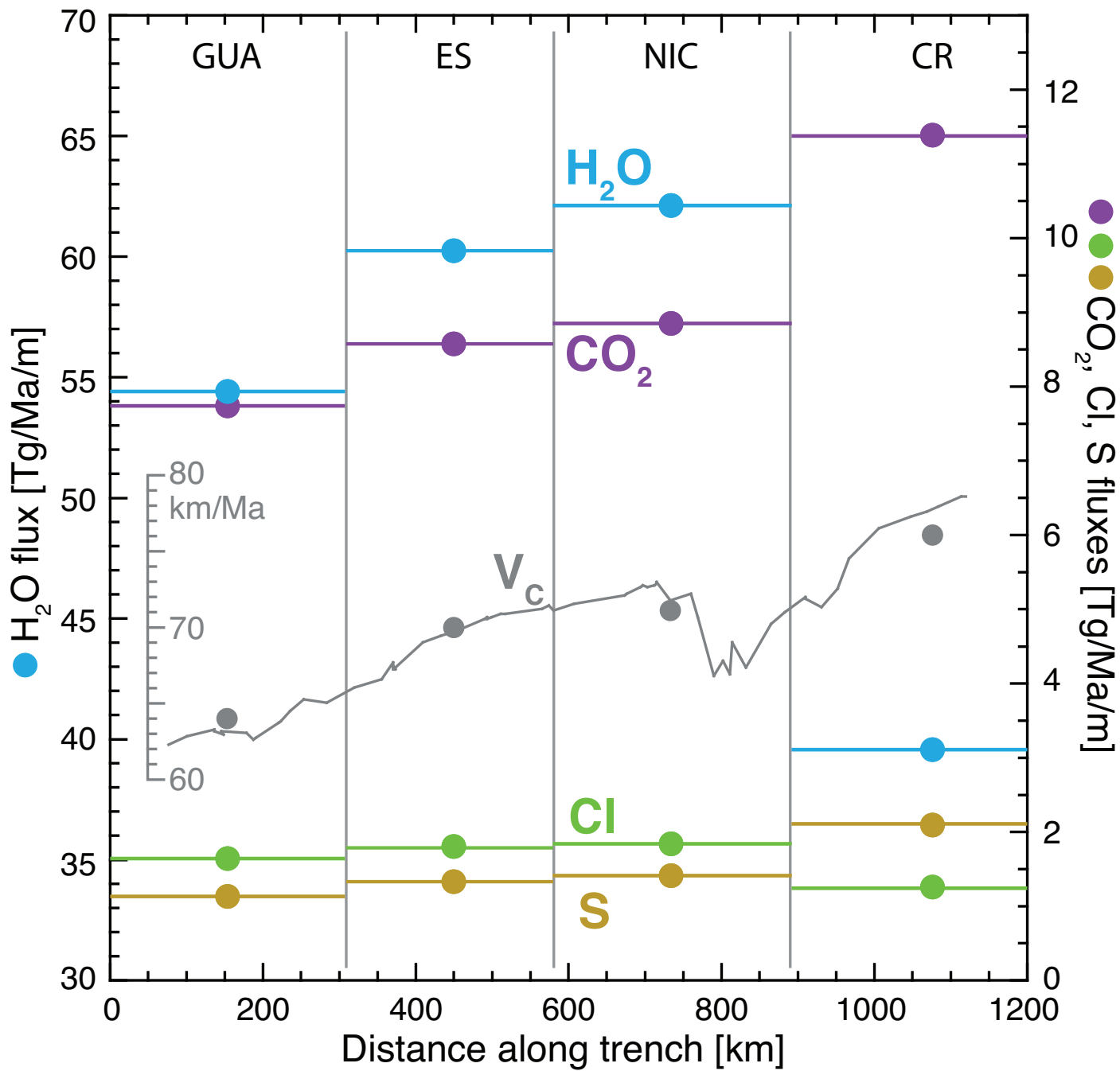


Figure 4
[Click here to download Figure: Fig4.eps](#)

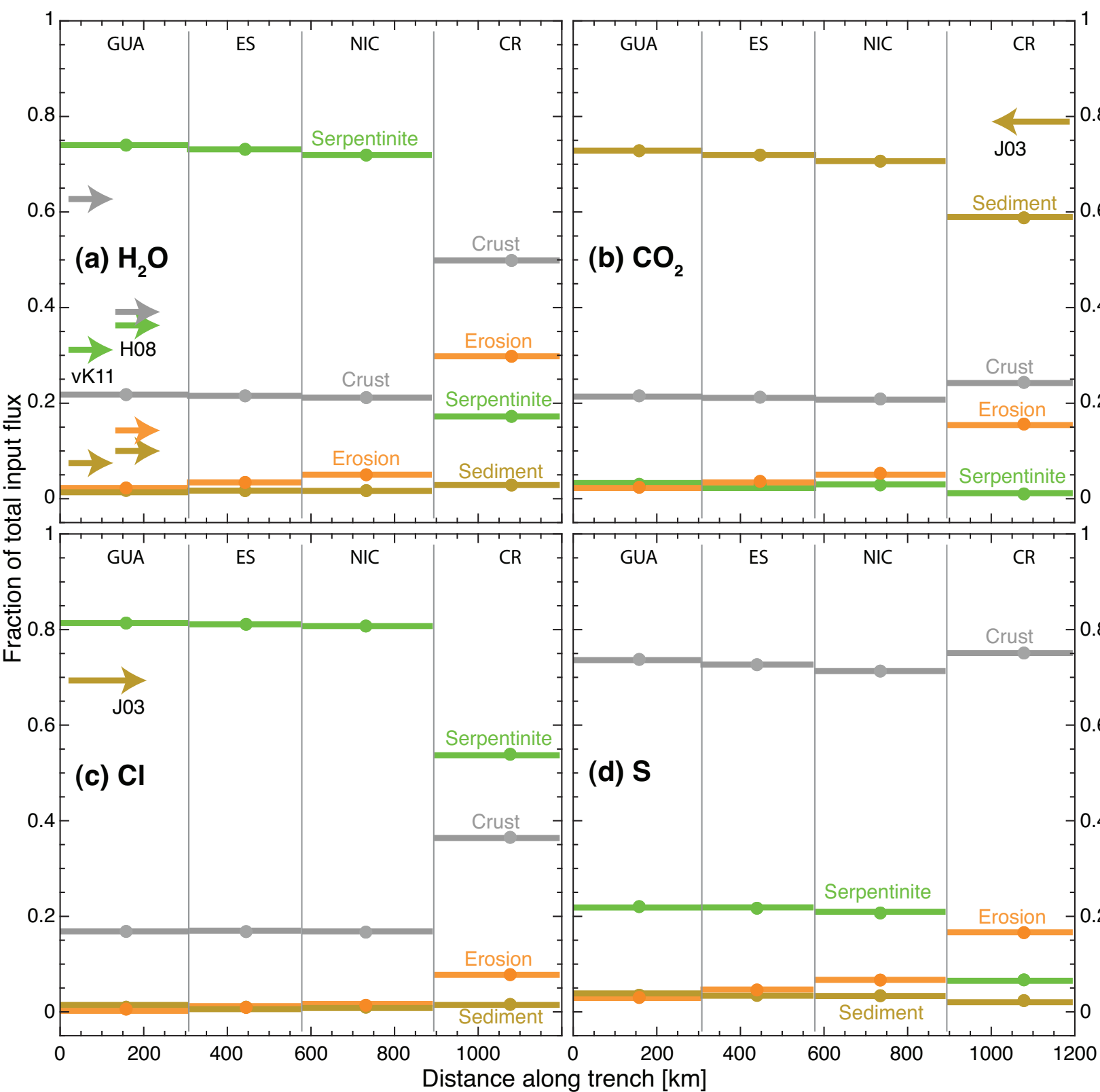


Figure 5
[Click here to download high resolution image](#)

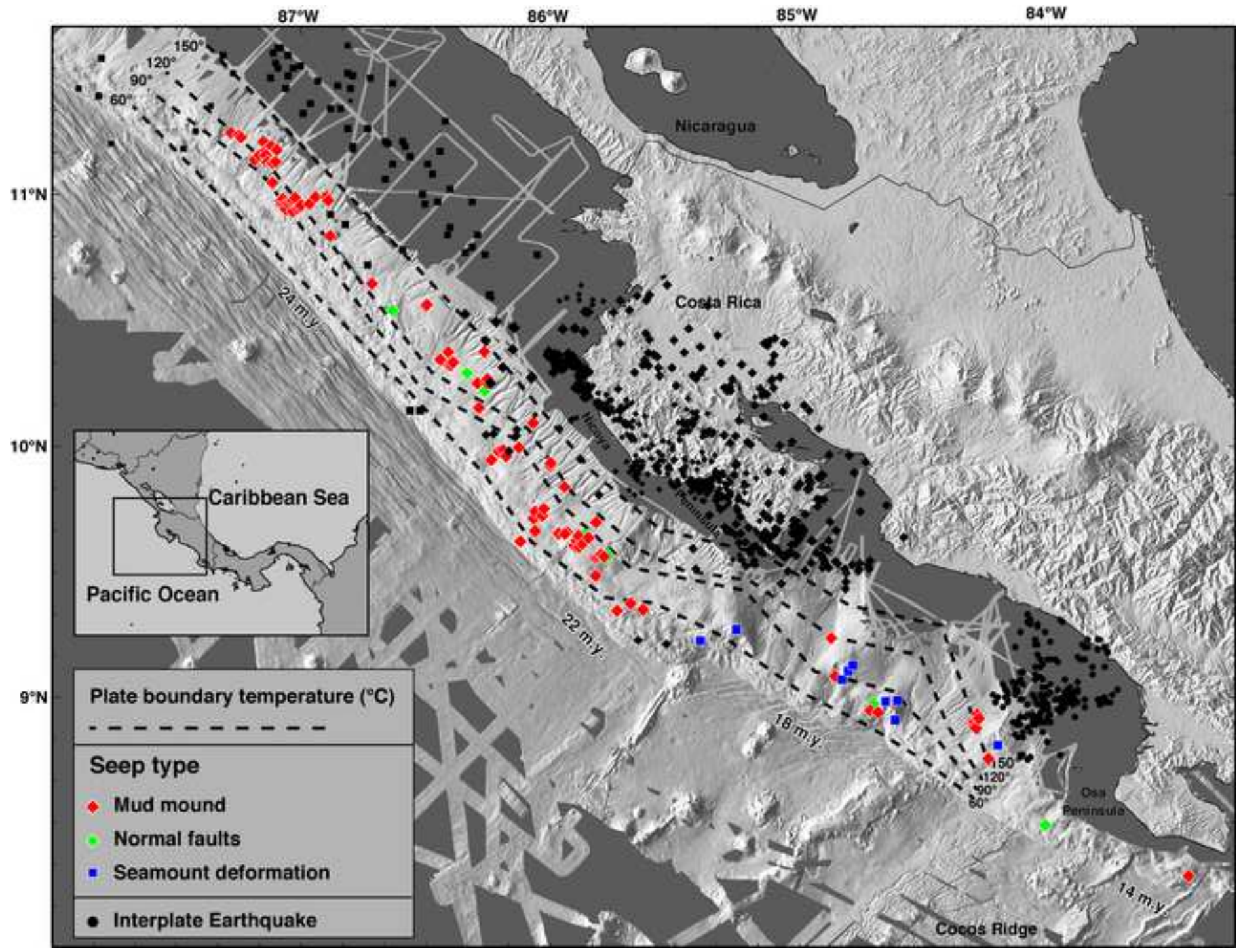


Figure 6

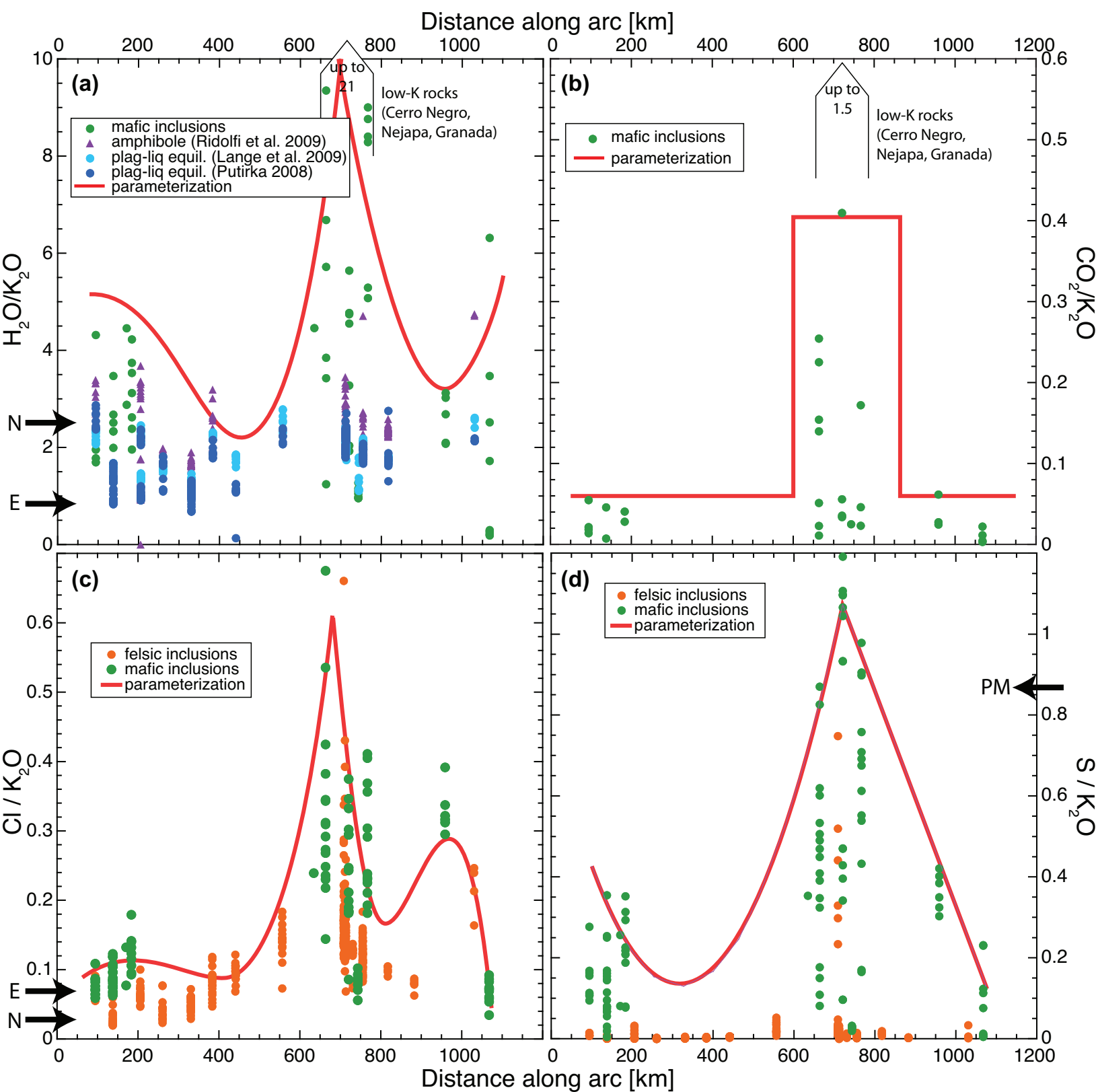
[Click here to download Figure: Fig6.eps](#)

Figure 7
[Click here to download Figure: Fig7.eps](#)

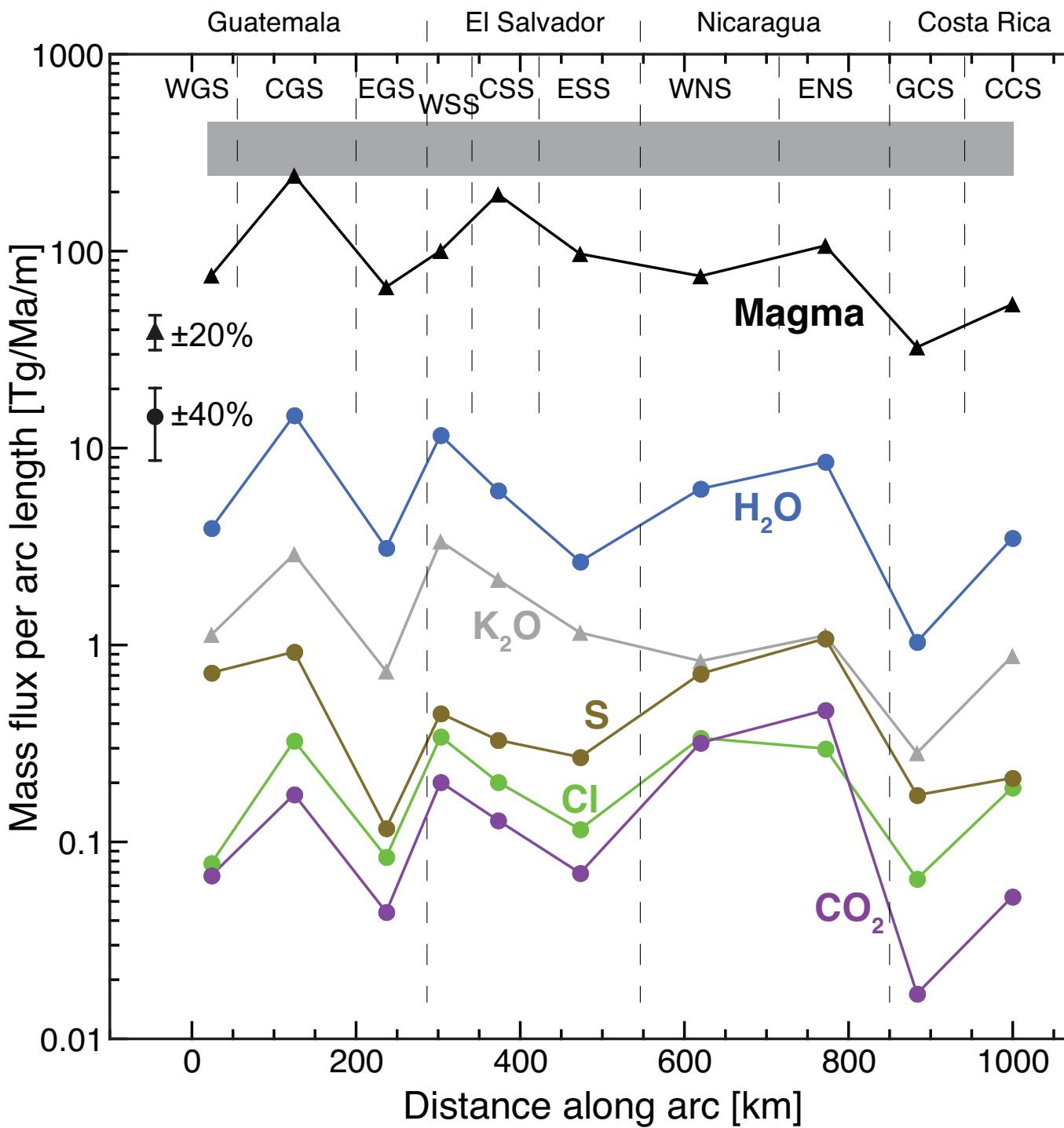


Figure 8
Click here to download Figure: Fig8.eps

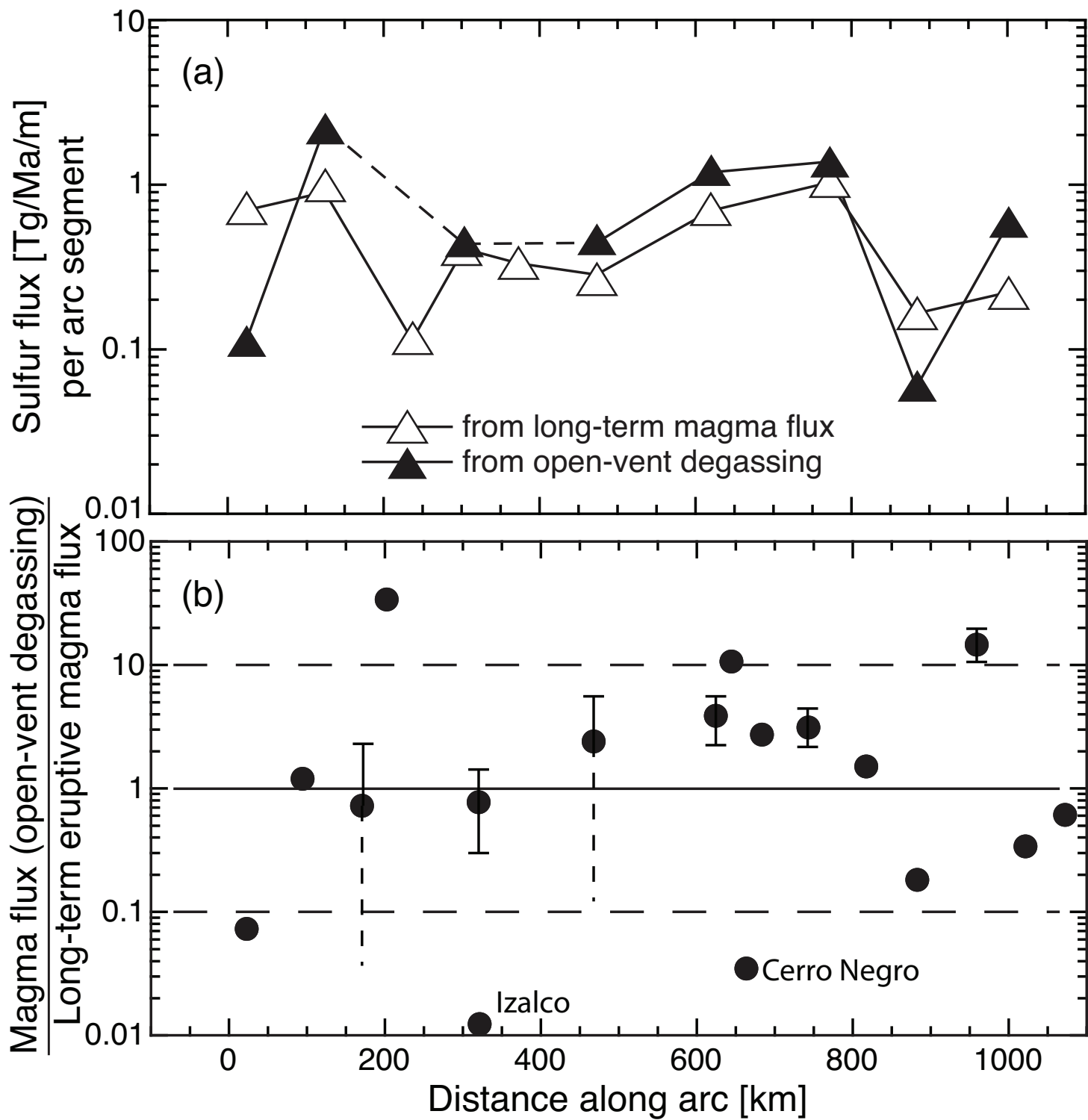


Figure 9

[Click here to download Figure: Fig9.eps](#)

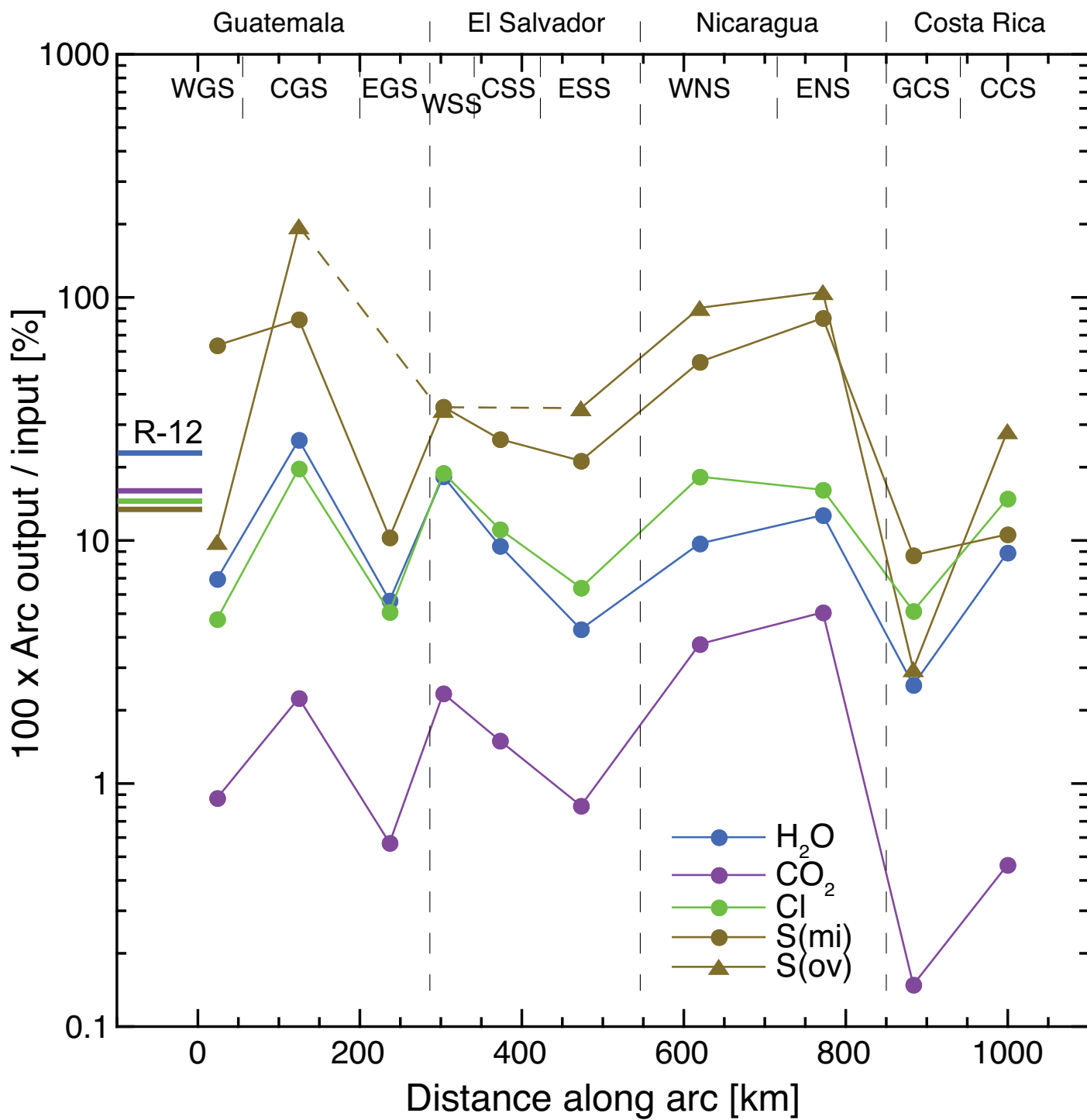


Figure 10
[Click here to download high resolution image](#)

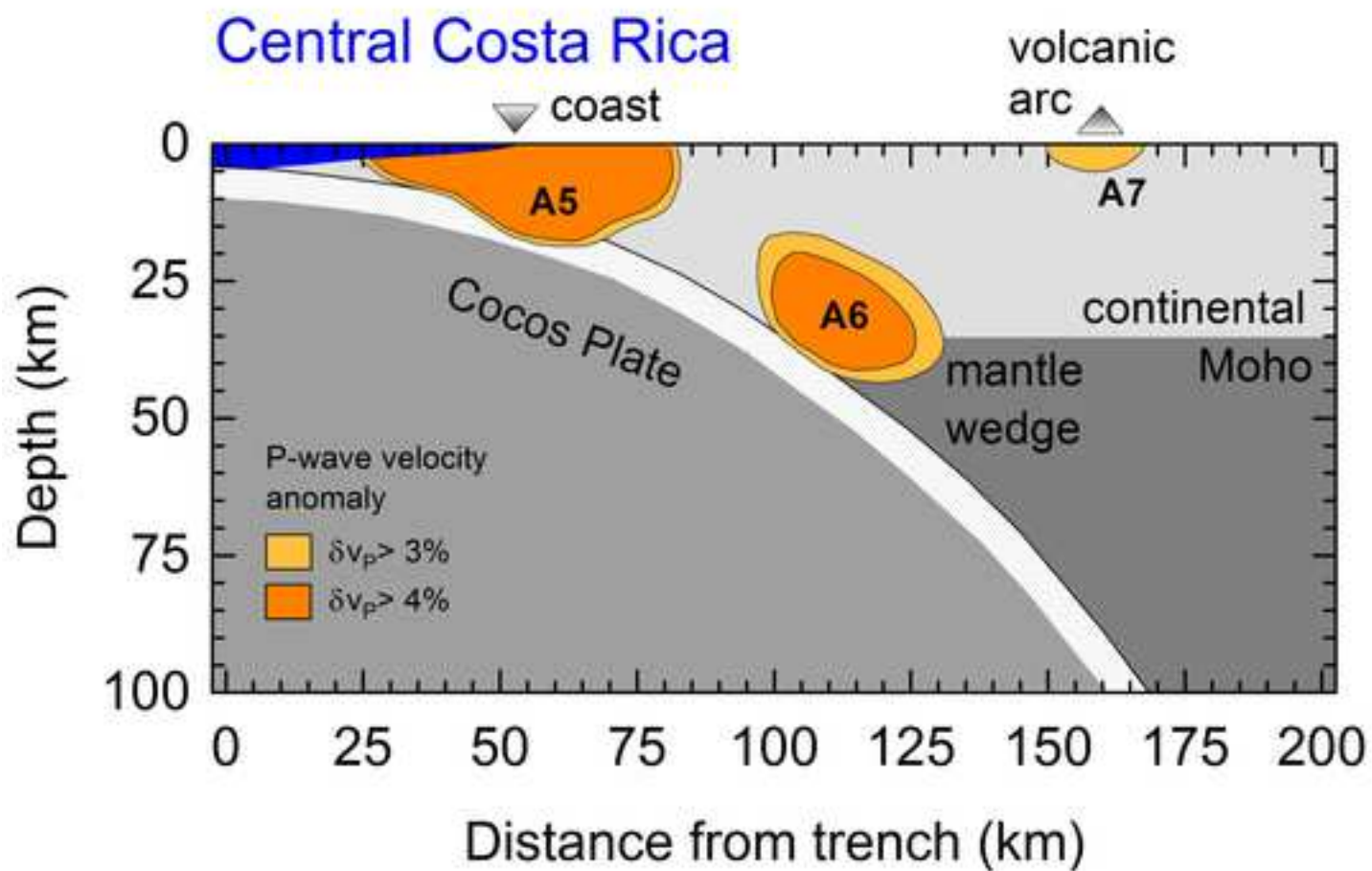
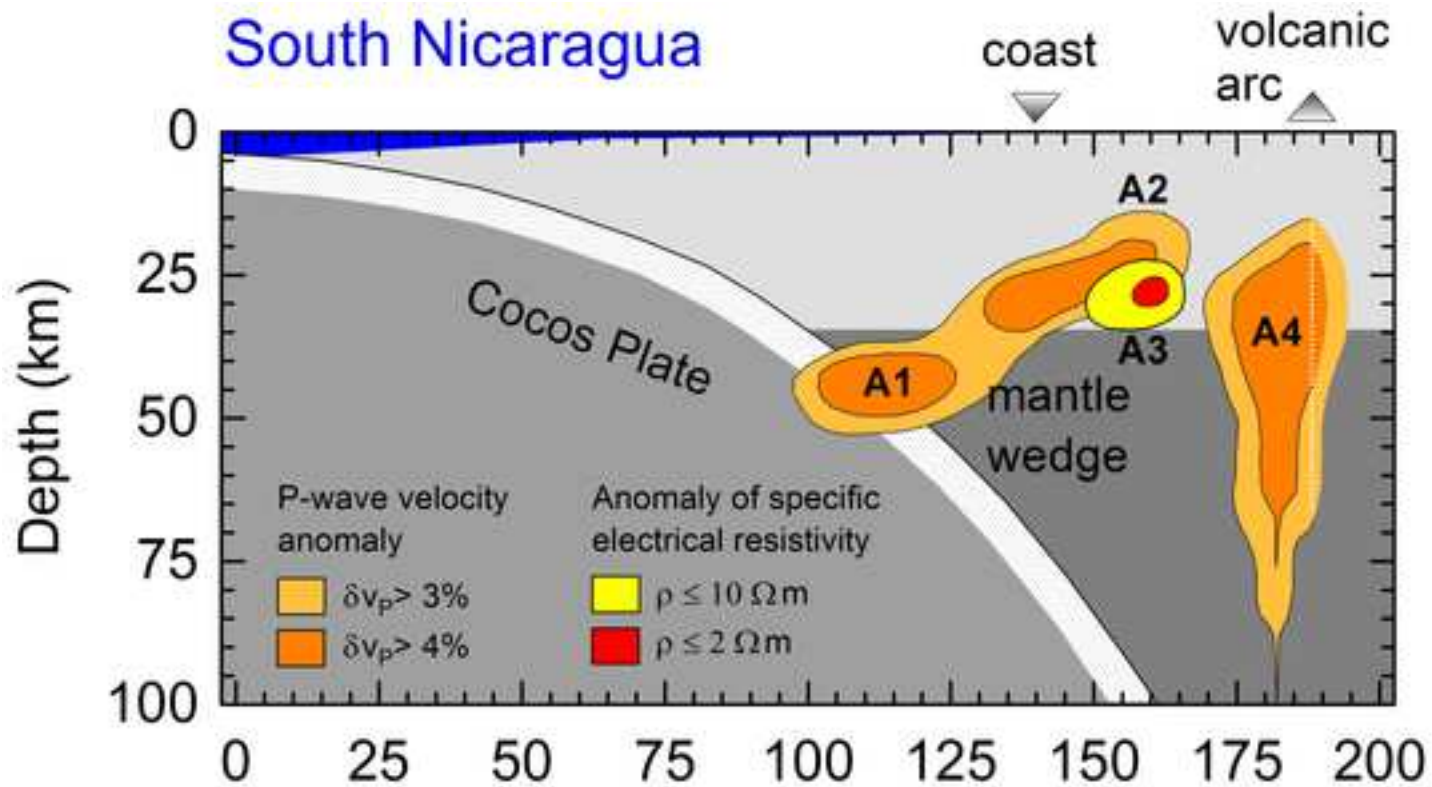


Figure 11
[Click here to download Figure: Fig11.eps](#)

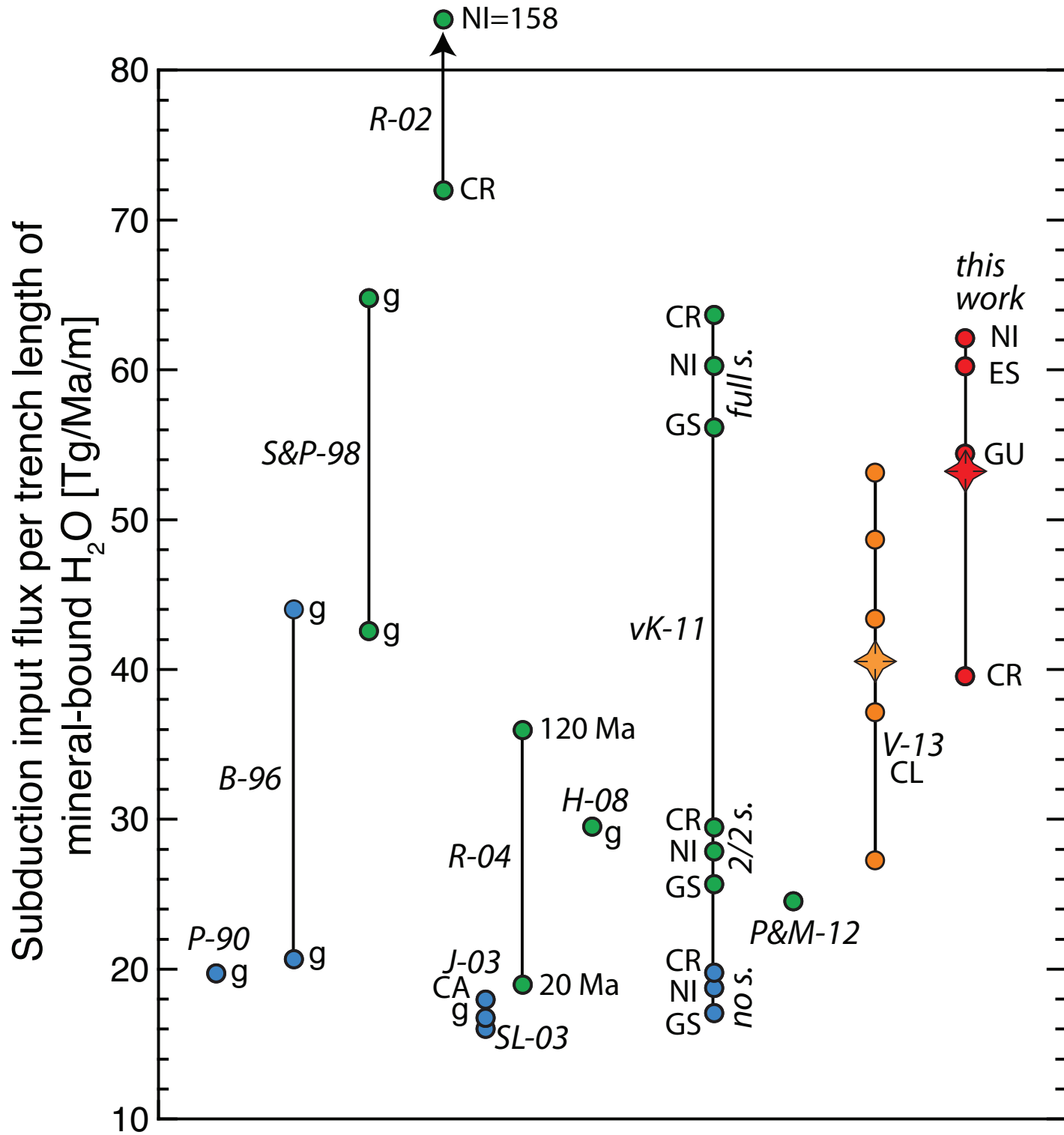


Figure 12
[Click here to download Figure: Fig12.eps](#)

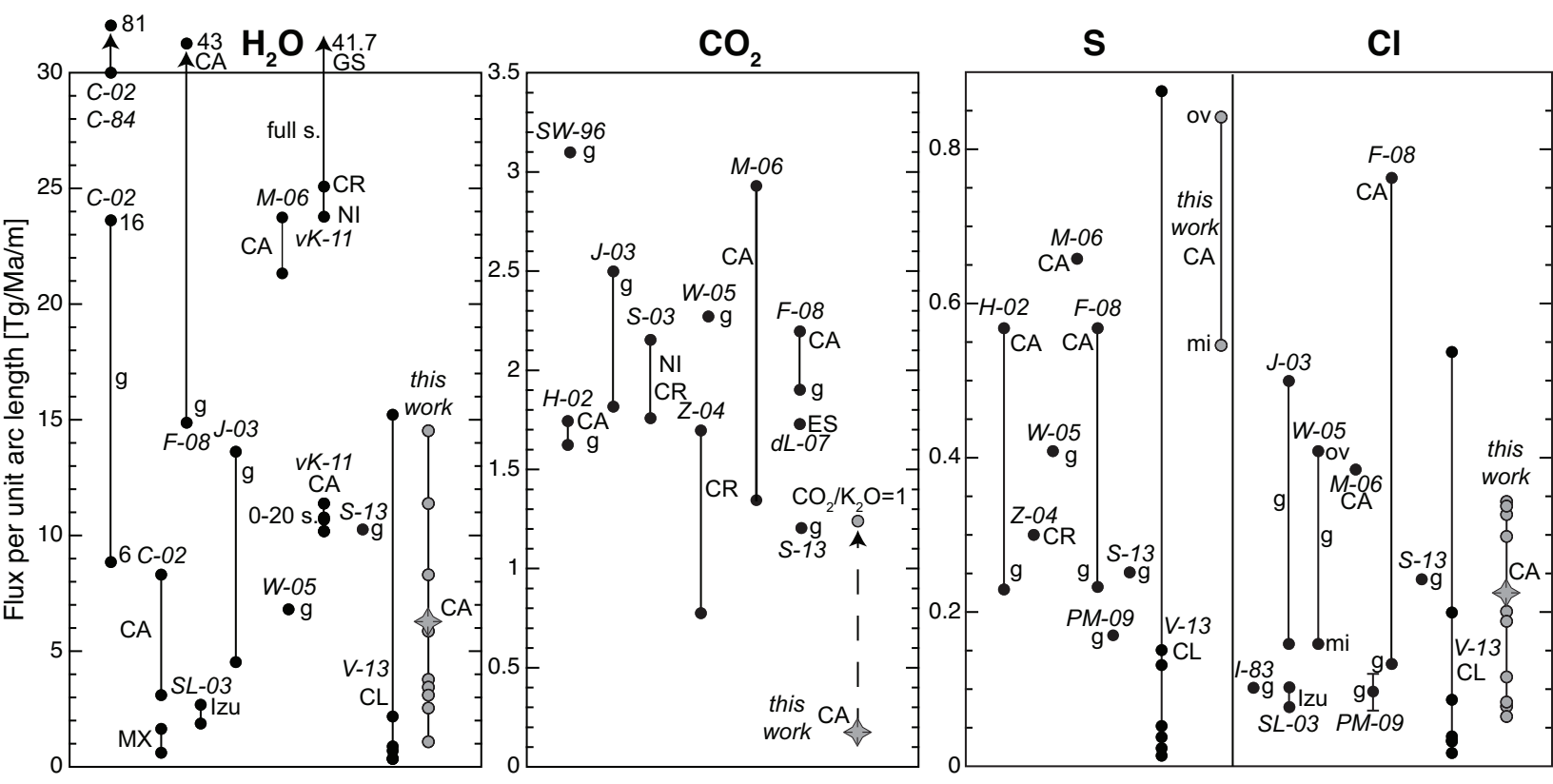


Table 1

Segment	Length km	Vc km/Ma	Thickness m	Density kg/m ³	Volatile Concentrations				Volatile Fluxes				
					H2O wt%	CO2 wt%	Cl wt%	S wt%	H2O Tg/Ma/m	CO2 Tg/Ma/m	Cl Tg/Ma/m	S Tg/Ma/m	
Sediments													
GUA	309	64	400	1620	4.59	26.55	0.0805	0.19	0.98	5.65	0.02	0.04	
ES	268	70	400	1620	4.59	26.55	0.0805	0.19	1.07	6.18	0.02	0.04	
NIC	314	71	400	1620	4.59	26.55	0.0805	0.19	1.08	6.27	0.02	0.04	
CR	374	76	400	1620	4.59	26.55	0.0805	0.19	1.16	6.71	0.02	0.05	
Cocos Crust													
			Thickness m	Density kg/m ³	H2O wt%	CO2 wt%	Cl wt%	S wt%	H2O Tg/Ma/m	CO2 Tg/Ma/m	Cl Tg/Ma/m	S Tg/Ma/m	
GUA			5000	2930	1.28	0.18	0.03	0.1	11.89	1.67	0.28	0.93	
ES			5000	2930	1.28	0.18	0.03	0.1	13.01	1.83	0.30	1.02	
NIC			5000	2930	1.28	0.18	0.03	0.1	13.19	1.86	0.31	1.03	
CR			7000	2930	1.28	0.18	0.03	0.1	19.77	2.78	0.46	1.54	
Serpentinized Mantle													
			Thickness m	Density kg/m ³	H2O wt%	CO2 wt%	Cl wt%	S wt%	H2O Tg/Ma/m	CO2 Tg/Ma/m	Cl Tg/Ma/m	S Tg/Ma/m	
GUA			7000	3000	3	0.02	0.1	0.02	40.32	0.27	1.34	0.27	
ES			7000	3000	3	0.02	0.1	0.02	44.10	0.29	1.47	0.29	
NIC			7000	3000	3	0.02	0.1	0.02	44.73	0.30	1.49	0.30	
CR			3000	3000	1	0.02	0.1	0.02	6.84	0.14	0.68	0.14	
Subduction Erosion													
			Erosion rate km ³ /Ma/km	Mass flux Tg/Ma/m	Density kg/m ³	H2O wt%	CO2 wt%	Cl wt%	S wt%	H2O Tg/Ma/m	CO2 Tg/Ma/m	Cl Tg/Ma/m	S Tg/Ma/m
GUA			12	35.16	2930	3.57	0.54	0.03	0.1	1.26	0.19	0.01	0.04
ES			20	58.60	2930	3.57	0.54	0.03	0.1	2.09	0.32	0.02	0.06
NIC			30	87.90	2930	3.57	0.54	0.03	0.1	3.14	0.47	0.03	0.09
CR			113	331.09	2930	3.57	0.54	0.03	0.1	11.82	1.79	0.10	0.33
					Total Volatile Composition				Total Volatile Fluxes				
					H2O wt%	CO2 wt%	Cl wt%	S wt%	total H2O Tg/Ma/m	total CO2 Tg/Ma/m	total Cl Tg/Ma/m	total S Tg/Ma/m	
GUA					83.78	11.94	2.54	1.95	54.44	7.78	1.65	1.27	
ES					83.79	11.95	2.52	1.96	60.27	8.62	1.81	1.41	
NIC					83.79	11.96	2.49	1.97	62.14	8.89	1.85	1.46	
CR					72.98	21.01	2.34	3.79	39.59	11.41	1.27	2.06	
Weighted mean entire subduction zone					81.15	14.17	2.47	2.41	53.20	9.31	1.62	1.58	

Table 2

Arc Segment	Length (km)	Magma (Tg/Ma/m)	K2O (Tg/Ma/m)	H2O (Tg/Ma/m)	CO2 (Tg/Ma/m)	Cl (Tg/Ma/m)	S (mi) (Tg/Ma/m)	S (ov) (Tg/Ma/m)
Western Guatemala segment	55	75.53	1.13	3.83	0.07	0.08	0.72	0.10
Central Guatemala segment	145	242.16	2.91	14.30	0.17	0.33	0.93	2.37
Eastern Guatemala segment	85	65.60	0.74	3.12	0.04	0.08	0.12	
W - Salvadorian segment	62	100.51	3.36	11.32	0.20	0.34	0.45	0.44
C - Salvadorian segment	78	194.23	2.15	5.80	0.13	0.20	0.33	
E - Salvadorian segment	121	96.97	1.16	2.60	0.07	0.12	0.27	0.45
Western Nicaraguan segment	166	74.57	0.83	6.02	0.33	0.34	0.71	1.23
Eastern Nicaraguan segment	137	106.78	1.12	8.07	0.45	0.30	1.08	1.33
Guanacaste segment	92	32.49	0.28	1.02	0.02	0.07	0.17	0.06
Cordillera Central segment	150	53.89	0.88	3.51	0.05	0.19	0.21	0.53
Mean total CAVA	1091	106.38	1.38	6.18	0.17	0.22	0.54	0.83
Arc output relative to input at trench				%	%	%	%	%
Western Guatemala segment				7.03	0.87	4.74	63.56	9.87
Central Guatemala segment				26.26	2.25	19.81	81.27	196.67
Eastern Guatemala segment				5.73	0.57	5.08	10.32	
W - Salvadorian segment				18.78	2.35	18.98	35.53	34.50
C - Salvadorian segment				9.62	1.50	11.12	26.08	
E - Salvadorian segment				4.32	0.81	6.41	21.32	35.08
Western Nicaraguan segment				9.68	3.75	18.32	54.38	90.58
Eastern Nicaraguan segment				12.99	5.07	16.17	82.29	105.32
Guanacaste segment				2.59	0.15	5.13	8.70	2.96
Cordillera Central segment				8.87	0.46	14.88	10.61	28.27
Mean total CAVA				10.08	1.99	12.15	41.36	63.78